Efficient inversion of the cone beam transform for a general class of curves

by

Mikhail Kapralov
B.Sc. St. Petersburg State University, St. Petersburg, Russia

A thesis submitted in partial fulfillment of the requirements
for the degree of Master of Science
in the Mathematics
in the College of Sciences
at the University of Central Florida
Orlando, Florida

Spring Term
2007

Major Professor: Alexander Katsevich

ABSTRACT

Image reconstruction from projections is important both in pure mathematics (as a problem of integral geometry) and in applications (as a problem of computed tomography (CT)). Cone beam CT is one of the most common medical imaging modalities. Here one recovers a function $f(x), x \in \mathbb{R}^3$, knowing the integrals of f along lines that intersect a curve C. The curve C is usually called a source trajectory. The ever-increasing needs of medical imaging require the development of inversion algorithms for more and more general source trajectories.

A number of theoretically exact algorithms have been proposed in the past several years. They can be classified into three groups: filtered backprojection (FBP) algorithms, slow-FBP algorithms, and backprojection filtration (BPF) algorithms. Slow-FBP and BPF algorithms are quite flexible, allow some transverse data truncation, and can be used for virtually any complete source trajectory [PN05, PNC05, ZPXW05, SZP05, YZYW05b, YZYW05a, ZLNC04]. FBP algorithms are less flexible, but they are by far the fastest and have been developed for a range of source trajectories. They include constant pitch helix [Kat02a, Kat04b, Kat04c, Kat06], dynamic pitch helix [KBH04, KK06a], circle-and-line [Kat04a], circle-and-arc [Kat05, CZLN06], and saddle [YLKK06]. Significant progress has also been achieved in the development of quasi-exact algorithms [BKP05, KBK06].

As the list presented above shows, until now FBP algorithms have been proposed only for certain types of well-defined trajectories: helices, saddles, etc. The goal of the thesis was

to obtain a deeper understanding of the properties that a curve C needs to have to admit an FBP-type reconstruction algorithm and develop reconstruction algorithms for more general source trajectories.

In the first chapter we develop a reconstruction algorithm for the dynamic pitch helical trajectory. Such a trajectory is important in many clinical applications, e.g. bolus chasing, whole body scans, etc. The first investigation of dynamic pitch trajectories was presented in [YZW04b]. The first exact FBP algorithm was proposed in [KBH04] under the convexity condition, i.e. $v(s) + a'(s)$ does not change sign. Here v and a are the axial velocity and acceleration of the source (relative to the patient), respectively. Technologically it is much more difficult to maintain a smooth dynamic velocity profile compared with maintaining a constant table speed. Thus one might expect that the above condition can be violated in real scans. In this chapter we study what happens in this case and obtain an exact FBP reconstruction algorithm, which is applicable in some region inside the helix. The region does not extend all the way to the helix, and its size depends on the severity of the violation. If the violation is not very strong, then the region is sufficiently large. In real CT scanners gantries have an opening, which is only a fraction of the distance from the axis of rotation to the source. Thus our results imply that artifact-free exact image reconstruction is possible whithin the entire field of view of CT scanners even when the convexity condition is violated. Only the case of a single localized violation of the convexity condition is considered. Our results apply also in the case of multiple violations that are sufficiently far apart. The results obtained in chapter 1 have been published in [KK06a].

In the second chapter we consider the following problem. As the discussion above shows, there no FBP algorithm was developed for a general class of curves. Ideally, such a class would be described only in terms of some basic geometric properties (e.g., smoothness, curvature, etc.) rather than specifying the types of curves (helices, etc.). We develop a theoretically exact shift-invariant FBP algorithm for a wide class of source trajectories. The conditions describing our class are very natural. We consider curves C that are smooth, have no self-intersections, have positive curvature and torsion, do not bend too much, and do not admit lines which are tangent to C at one point and intersect C at another point. Our algorithm applies to any curve with these properties. The inversion algorithm obtained here is a generalization of the formula proposed for constant- and variable-pitch helices in [Kat02a, Kat04b, KBH04].

The importance of our results is two-fold. First, the algorithm can be used in a variety of applications. For example, in electron-beam CT/micro-CT there arise source trajectories that can be described as helices with variable radius and pitch [YZW04a]. No efficient FBP algorithm existed for such curves, but the new one does apply. Nice first steps towards adapting the inversion formula of [Kat02a, Kat04b, KBH04] to these curves were obtained in [YZW04a]. Second, the results have theoretical value as well. They provide a deeper understanding of the available algorithms, put them into the context of a more general approach, and demonstrate which geometrical properties the curve is required to have for the FBP algorithm to apply. The results obtained in chapter 2 have been submitted for possible publication – [KK06b].

ACKNOWLEDGMENTS

I would like to thank my advisor Dr. Alexander Katsevich, who has been a most inspiring mentor, for his guidance during my work on the thesis, Dr. Mourad Ismail for his help and advice throughout my time at UCF and Dr. Alexandru Tamasan for serving on my dissertation committee.

TABLE OF CONTENTS

LIST OF FIGURES

LIST OF TABLES

VARIABLE PITCH HELIX VIOLATING THE CONVEXITY CONDITION

This chapter is organized as follows. In section 1.1 we describe the inversion algorithm of [Kat02b], which is the starting point of the new development, and describe a class of trajectories that violate the convexity condition. In section 1.2 we determine the domain $U_{PI} \subset U$ such that any $x \in U_{PI}$ admits a unique PI line. In sections 1.3 and 1.4 we impose some additional constraints on points $x \in U_{PI}$ that will simplify the derivation of backprojection coefficients, and define the set of points $U_0 \subset U_{PI}$ satisfying all the constraints. The main tool here is the analysis of diagrams, which was proposed in [Kat06]. An exact shift-invariant FBP algorithm for reconstruction inside U_0 is derived in section 1.5. The results of numerical experiments are presented in section 1.6. Finally, some technical proofs are collected in the Appendix.

1.1 Convexity condition and its violation

First we introduce the notation. Consider the following generalized helical source trajectory:

$$C := \{y \in \mathbb{R}^3 : \; y_1 = \cos s, y_2 = \sin s, y_3 = \psi(s), s \in \mathbb{R}\}, \tag{1.1}$$

where $\psi(s) \in C^2(\mathbb{R})$ and $\dddot{\psi}(s)$ is piecewise continuous. Here and below we use the convention that the derivatives with respect to s are denoted by dots. All other derivatives are denoted by primes.

Even though (1.1) represents the case when the gantry is perpendicular to the axis of rotation, our results apply to the tilted gantry as well. Consider, for example, the gantry tilted about the x_1-axis. Then the equation of the helix becomes

$$\tilde{C} = \{y \in \mathbb{R}^3 : \, y_1 = \cos s, y_2 = \cos\mu \sin s, y_3 = \psi(s) + \sin\mu \sin s, s \in \mathbb{R}\}, \tag{1.2}$$

where μ is tilt angle. Denoting $\psi_1(s) := \psi(s) + \sin\mu \sin s$ and changing variables $y_2' = y_2/\cos\mu$ (which maps any rectangular grid parallel to the coordinate axes to another such grid), we obtain an equation of the type (1.1).

Let U be an open set strictly inside the helix:

$$\bar{U} \subset \{x \in \mathbb{R}^3 : \, x_1^2 + x_2^2 < 1\}. \tag{1.3}$$

The cone beam transform of a function $f \in C_0^\infty(U)$ is

$$D_f(y, \Theta) := \int_0^\infty f(y + \Theta t)dt, \Theta \in S^2, \tag{1.4}$$

where S^2 is the unit sphere in $\mathbb{R}^3$. Furthermore, $\beta(s, x)$ denotes the unit vector that points to x from $y(s)$

$$\beta(s, x) = \frac{x - y(s)}{|x - y(s)|}, \; x \in U, \; y(s) \in C. \tag{1.5}$$

Given two values $s_1, s_2 \in \mathbb{R}$, $H(s_1, s_2)$ denotes the chord with endpoints $y(s_1), y(s_2) \in C$.

$\Pi_{osc}(s)$ is the osculating plane to C at $y(s)$, which is the plane containing $y(s)$ and parallel to $\dot{y}(s), \ddot{y}(s)$. When the source is at $y(s)$, the corresponding detector plane is denoted by $DP(s)$. L_0 is the line on $DP(s)$, which is the intersection of $\Pi_{osc}(s)$ and $DP(s)$. We denote the projections of the lower and upper turns of the helix onto $DP(s)$ by Γ_- and

Γ_+, respectively. For $x \in U$, $I_{PI}(x) = [s_b(x), s_t(x)]$ denotes the PI-parametric interval of x, $C_{PI}(x)$ is the corresponding section of the helix, and $L_{PI}(x)$ denotes the PI line of x.

For convenience of the reader we describe briefly the inversion formula for a constant pitch helix proposed in [Kat02b]. Let $e_0(s,x)$ denote the unit vector in the plane through $y(s)$ and spanned by $\beta(s,x)$ and $\dot{y}(s)$ subject to the conditions $e_0(s,x) \cdot \beta(s,x) = 0$ and $e_0(s,x) \cdot \dot{y}(s) > 0$. Given $y(s)$, $s \in (s_b(x), s_t(x)) \backslash \{s_0(x)\}$, one can find $s_{tan} \in I_{PI}(x)$, $s_{tan} \neq s$, such that the plane through x, $y(s)$ and $y(s_{tan})$ is tangent to $C_{PI}(x)$ at $y(s_{tan})$. Here $s_0(x) \in I_{PI}(x)$ is the value such that $\Pi_{osc}(s_0(x))$ contains x. For the exceptional values of $s \in \{s_b(x), s_t(x), s_0(x)\}$, s_{tan} is determined by continuity. This construction defines a continuous function $s_{tan} = s_{tan}(s,x)$. One can show that $s = s_0(x)$ implies $s_{tan} = s_0(x)$. Now let $e_1(s,x)$ be a unit vector in the plane through $x, y(s)$ and tangent to C at $y_{tan}(s)$. We require additionally $e_1(s,x) \cdot \beta(s,x) = 0$. This defines a continuous vector-valued function $e_1(s,x)$ up to a sign. Finally, the ambiguity is eliminated by requiring that $e_0(s,x) = e_1(s,x)$ when $s = s_{tan} = s_0(x)$.

The inversion formula of [Kat02b] can be written in the form

$$\begin{aligned} f(x) = -\frac{1}{2\pi^2} \int_{I_{PI}(x)} \sum_{k=0}^{M(s)} \frac{c_k(s)}{|x - y(s)|} \\ \times \int_0^{2\pi} \frac{\partial}{\partial q} D_f(y(q), \cos\gamma\beta(s,x) + \sin\gamma e_k(s,x))|_{q=s} \frac{d\gamma}{\sin\gamma} ds, \ k = 0, 1, \end{aligned} \tag{1.6}$$

where $f \in C_0^\infty(U)$, $M(s) = 1$, and $c_0(s) = c_1(s) = 1/2$ for all $s \in I_{PI}(x)$. Here c_k's are the *b*ackprojection coefficients, i.e. the coefficients used to sum up the contributions from different filtering lines on the detector plane.

As was already mentioned, (1.6) was derived for constant-pitch helices. It was shown in [KBH04] that the improved inversion formula of [Kat02a] is applicable also to variable-pitch helices (1.1) provided that $\mu(s) = \dot{\psi}(s) + \dddot{\psi}(s)$ is positive (or, negative) almost everywhere (a.e.). This requirement was called the "convexity condition" in [KBH04]. One easily sees that the same argument as in [KBH04] can be used to show that the original inversion formula (1.6) is also applicable as long as the convexity condition holds. For simplicity, here and everywhere below we assume that $\mu(s)$ is positive a.e. whenever the convexity condition holds.

As a side remark let us mention that a simple calculation gives $\mu(s) = C(s)\tau(s)$, where $C(s) > 0$ and $\tau(s)$ is the torsion of the source trajectory. Thus the convexity condition

$$\mu(s) > 0 \quad \text{a.e.} \tag{1.7}$$

can be reformulated as $\tau(s) > 0$ a.e.

Now suppose that the convexity condition is violated over an interval $[A, B]$. More precisely,

$$\mu(s) < 0, s \in (A, B);\ \mu(s) > 0, s \notin [A, B]. \tag{1.8}$$

We also assume that the violation of (1.7) is not too strong in the sense that will be made clear in sections 1.2 and 1.4. As was shown in [KBH04], if (1.7) holds then almost any plane through any $x \in U$ can have only one or three intersections with $C_{PI}(x)$. It turns out that the violation of condition (1.7) leads to the formation of an exceptonal set $U_{5IP} \subset U$ (cf. Section 1.6). For any $x \in U_{5IP}$ there are planes through x that intersect $C_{PI}(x)$ at five

points. Hence (1.6) is no longer applicable for image reconstruction in U_{5IP}. Consequently, the original 1PI algorithm needs to be modified in order to account for the exceptional set.

1.2 The region where PI lines are unique

Existence and uniqueness of PI lines is a necessary condition for (1.6) to hold. Thus, our first goal is to determine the region $U_{PI} \subset U$ where PI lines are unique. The existence of PI lines for all $x \in U$ follows immediately from a standard argument (see e.g. [KL03]). Local uniqueness of PI lines implies that the following map is invertible:

$$(s_b, s_t, \lambda) \to x = y(s_b) + \lambda(y(s_t) - y(s_b)), 0 < s_t - s_b < 2\pi, 0 < \lambda < 1. \tag{1.9}$$

Here $y(s_b)$ and $y(s_t)$ are the endpoints of a PI line, and λ is the parameter along the line. Since the existence of a local inverse is equivalent to the Jacobian matrix being nondegenerate, we obtain the condition:

$$[y(s_t) - y(s_b), \dot{y}(s_b), \dot{y}(s_t)] \neq 0 \quad \forall s_b, s_t \in \mathbb{R}, 0 < s_t - s_b < 2\pi, \tag{1.10}$$

where the brackets denote the triple product: $[a, b, c] := a \cdot (b \times c)$.

As was shown in [KBH04], PI lines are unique as long as $\mu(s) > 0$ a.e. If the convexity condition is violated, then (1.10) fails for certain chords. We call such chords *c*ritical. Our goals are to determine the region where PI lines fail to be unique and also verify that the region of non-uniqueness depends continuously on μ.

First we establish that the critical chords depend continuously on μ. Denote

$$\mu_\varepsilon(s) = \mu(s) + \varepsilon\eta(s), \tag{1.11}$$

where $\eta(s)$ is a compactly supported function, and $\mu(s)$ satisfies (1.8). Let $\phi(s)$ be the solution of the differential equation

$$\dot{\phi}(s) + \dddot{\phi}(s) = \eta(s), \tag{1.12}$$

such that $\dot{\phi}(s) \equiv 0$ outside of $\operatorname{supp}\eta$. As is easily checked, such a solution exists if $\int \eta(s)\cos s ds = \int \eta(s)\sin s ds = 0$.

Define, $\psi(s,\varepsilon) := \psi(s) + \varepsilon\phi(s)$. Thus $\varepsilon\phi(s)$ describes a compactly supported perturbation of the original source trajectory. By construction, $\dot{\psi}(s,\varepsilon) + \dddot{\psi}(s,\varepsilon) = \mu_\varepsilon(s)$. Since $\psi(s) = \psi(s,0)$, for convenience we write $\psi(s)$ instead of $\psi(s,\varepsilon=0)$. Clearly, $\psi'_\varepsilon(s,\varepsilon) = \phi(s)$. Denote

$$Q(s,l,\varepsilon) := [y(l)-y(s), \dot{y}(s), \dot{y}(l)] = \begin{vmatrix} \cos l - \cos s & \sin l - \sin s & \psi(l,\varepsilon) - \psi(s,\varepsilon) \\ -\sin s & \cos s & \dot{\psi}(s,\varepsilon) \\ -\sin l & \cos l & \dot{\psi}(l,\varepsilon) \end{vmatrix}. \tag{1.13}$$

The graph of $Q(0,l,\varepsilon=0)$ as a function of $l \in [-\pi,\pi]$ when $\psi(s) = s$ is shown in Fig. 1.1 below. The function $Q(0,l,0)$ is never zero for any l, $0 < |l| < 2\pi$.

Replacement of the standard helix with a variable-pitch helix, which satisfies (1.7), leads to a deformation of the graph. Since a new zero crossing would imply non-uniqueness of PI lines and thus contradict the results of [KBH04], the deformation does not introduce any new zero intersections inside $(-2\pi, 2\pi)$.

Let us calculate $Q(s,l,0)$ for the generalized helix. Substitution of $\varepsilon = 0$ into (1.13) gives

$$\begin{aligned} Q(s,l,0) &= (\psi(l)-\psi(s))\sin(s-l) + (\dot\psi(s)+\dot\psi(l))(1-\cos(l-s)) \\ &= (1-\cos(l-s))\left[\dot\psi(l)+\dot\psi(s) - (\psi(l)-\psi(s))\frac{\sin(l-s)}{1-\cos(l-s)}\right] \\ &= (1-\cos(l-s))G(l,s), \end{aligned} \tag{1.14}$$

where G is exactly the function that was introduced in [KBH04] (see eqn. (39)). Recall that (see eqns. (27), (28), and (42) in [KBH04]):

$$G(l,s) = \int_s^l \frac{\Phi(p,s)}{1-\cos(p-s)}dp,\ \ \Phi(p,s) = \int_s^p \mu(t)(1-\cos(t-s))dt. \tag{1.15}$$

From (1.14) and (1.15),

$$Q'_l(s,l,0) = \sin(l-s)G(l,s) + (1-\cos(l-s))G'(l,s). \tag{1.16}$$

If $l \neq s$ is such that $G(l,s) = Q(s,l,0) = 0$, then (1.16) and (1.15) imply

$$Q'_l(s,l,0) = (1-\cos(l-s))G'(l,s) = \int_s^l \mu(t)(1-\cos(t-s))dt. \tag{1.17}$$

In order to ensure that there are almost always either zero or two solutions $l \in (s-2\pi, s+2\pi)$ of $Q(s,l,0)=0$ for a fixed s and also to simplify the derivation in section 1.5, we introduce the following constraint on the severity of the violation:

Condition 1. *The are no critical chords $H(s_0,s_1)$ with $\pi \le s_1 - s_0 < 2\pi$.*

Now we study the shape of the graph of $Q(s,l,0)$. Suppose first that $s \in (A,B)$, i.e. $\mu(s) < 0$. Note that the signs of $Q(s,l,0)$ and $G(s,l,0)$ are the same as long as $0 < |s-l| < 2\pi$. From (1.15) and (1.8), $G'_l(s,l,0) < 0$ if $l > s$ and l is sufficiently close to

s, but becomes positive as l moves further away from s. Analogously, $G'_l(s,l,0) > 0$ if $l < s$ and l is sufficiently close to s and becomes negative as l moves further from s. Since $G(s, l = s, 0) = Q(s, l = s, 0) = 0$, we conclude that locally the graph of $Q(s,l,0)$ for a fixed $s \in (A,B)$ looks like the one shown in Fig. 1.2 (left panel).

Suppose now $s < A$ and s is sufficiently close to A. Using the same reasoning as above, one sees that since $\mu(s) > 0$, the graph of $Q(s,l,0)$ starts from the origin similarly to the graph in Fig. 1.1. However, $Q(s,l,0)$ then temporarily becomes negative to the right of s because $\mu(l) < 0$ on (A,B). Hence in this case the graph of $Q(s,l,0)$ locally looks like the one shown in Fig. 1.2 (right panel).

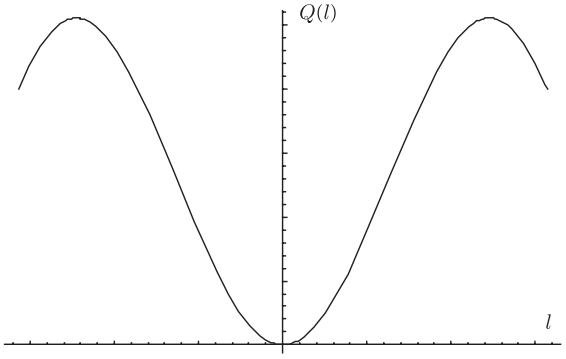

Figure 1.1: Graph of $Q(0,l,0)$ for the standard helix

Recall that $\mu(s)$ satisfies (1.8). Hence, in the limit $\varepsilon \to 0$, $Q(s,l,\varepsilon) = 0$ can only be satisfied in the following cases (up to a permutation of s and l):

I. $s \in [A,B]$, $l \le A$ or $l \ge B$

II. $s \le A$, $l \ge B$

So for a given s, which is sufficiently close to $[A, B]$ or inside $[A, B]$, there exist exactly two solutions l of $Q(s, l, \varepsilon) = 0$. In what follows we keep s fixed and denote any one of these solutions generically by $l(s, \varepsilon)$:

$$Q(s, l(s, \varepsilon), \varepsilon) = 0. \tag{1.18}$$

By construction, s and $l(s, \varepsilon)$ are the endpoints of a critical chord. We need to calculate l'_ε for each of the two cases listed above. By the implicit function theorem,

$$l'_\varepsilon = - \left. \frac{Q'_\varepsilon(s, l, \varepsilon)}{Q'_l(s, l, \varepsilon)} \right|_{l=l(s,\varepsilon),\varepsilon=0}. \tag{1.19}$$

Differentiating (1.13) with respect to ε and using that $\psi'_\varepsilon(s, \varepsilon) = \phi(s)$, we see that $Q'_\varepsilon(s, l, \varepsilon)$ is well-defined.

$Q'_l(s, l, 0)$ can also be easily estimated. From equation (1.17) and Figure 1.2 we see that $Q'_l(s, l, 0) < 0$ if $l = l_1(s, 0) < s$ and $Q'_l(s, l, 0) > 0$ if $l = l_2(s, 0) > s$ in Case I (see Figure 1.2, left panel) and $Q'_l(s, l, 0) < 0$ if $l = l_1(s, 0) < s$ and $Q'_l(s, l, 0) > 0$ if $l = l_2(s, 0) > s$ in Case II (see Figure 1.2, right panel). Our argument shows that generally the denominator in (1.19) is never zero provided that $s \neq l(s, 0)$. The denominator can become zero for some $l \neq s$ only for some critical values of s that belong to the regions $s < A$ or $s > B$. As is clear from Figure 1.2 (right panel), near these critical values of s the two roots $l_1(s, 0)$ and $l_2(s, 0)$ collide and disappear. Indeed, differentiating (1.13) we see that if $Q(s, l, 0) = Q'_l(s, l, 0) = 0$ for $l = l(s, 0)$, then $\Pi_{osc}(l(s, 0))$ touches C at $y(s)$. By analyzing the possible shapes of Γ_- and Γ_+ on $DP(l(s, 0))$ (see Figures 1.6 and 1.7 below), we see that $\Pi_{osc}(l(s, 0))$ cannot intersect the helix at any other point.

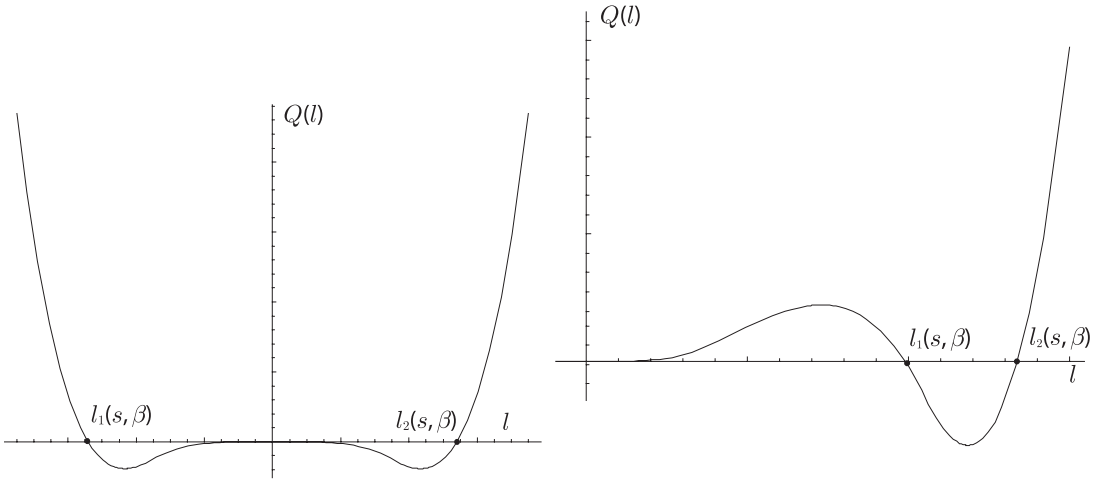

Figure 1.2: Graph of $Q(s, l, 0)$ for the case $s \in [A, B]$ (left panel) and $s < A$ (right panel).

It follows from the expression for $Q(s, l, 0)$ and the preceding argument that if the violation of the convexity condition is small, the critical chords are located close to the source trajectory.

Now we define $U_{PI} \subset U$ to be the largest connected set containing the x_3-axis and not intersecting any critical chords. If the violation (1.8) is not too strong (e.g., condition V1 holds), then U_{PI} is well-defined. It is easy to see that any $x \in U_{PI}$ admits a unique PI line. If it is not the case, find $x' \in U_{PI}$ with several PI lines and connect x' by a continuous path $x(t) \subset U_{PI}$ with $x'' \in U_{PI}$, which admits a single PI line. x'' exists, because we can take it sufficiently far from the violation (1.8). Since U_{PI} is connected, such a path exists. From (1.10), PI lines depend smoothly on x. On the other hand, somewhere along the path there must be a point $x(t^*)$ where a PI line of x disappears or PI lines of x merge. Then in a neighborhood of this point condition (1.10) is violated, and we get a contradiction with the assumption that the path is inside U_{PI}.

In this section we have shown that the boundary of the region U_{PI} where PI lines are unique is formed by the union of critical chords, whose endpoints can be parametrized in the form $s, l(s, \varepsilon = 0)$, and these chords depend continuously on μ. Critical chords form several surfaces and the boundary of U_{PI} is contained in the union of these surfaces. Fig. 1.3 shows the cross-section of these surfaces by the plane $x_3 = \psi(0)$ for a source trajectory that violates the convexity condition (see (1.34) below and Fig. 1.10).

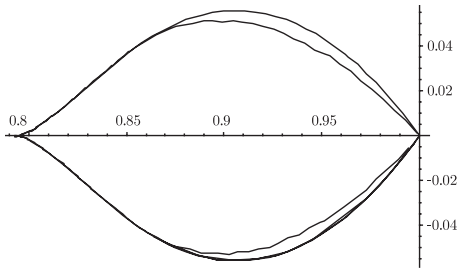

Figure 1.3: The boundary of U_{PI} derived in section 1.2 for a sample source trajectory

1.3 Analysis of diagrams - possible violations

We use here an auxiliary construction, which was introduced in [Kat06]. For a given point $x \in U_{PI}$ define two curves on the surface of the unit sphere S^2. The A-curve consists of all vectors orthogonal to $L_{PI}(x)$ (thus, the A-curve is in fact a great circle in S^2). The $T-$curve consists of the vectors

$$\alpha(s) = \pm \frac{(x - y(s)) \times \dot{y}(s)}{|(x - y(s)) \times \dot{y}(s)|}, \ s \in I_{PI}(x). \tag{1.20}$$

For each s, $\alpha(s)$ is the unit vector normal to the plane passing through x and tangent to C at $y(s)$. Following [Kat06], we represent these curves on the plane using spherical coordinates (θ_1, θ_2) defined by

$$S^2 \ni \alpha(s) = (\cos\theta_1 \sin\theta_2, \sin\theta_1 \sin\theta_2, \cos\theta_2), -\pi < \theta_1 < \pi, 0 < \theta_2 < \pi. \tag{1.21}$$

Also, as α and $-\alpha$ define the same plane, we restrict θ_1 to the interval $[0, \pi]$ by using the identification

$$(\theta_1, \theta_2) \cong ((\theta_1 + \pi)_{\mathrm{mod}\, 2\pi}, \pi - \theta_2) \tag{1.22}$$

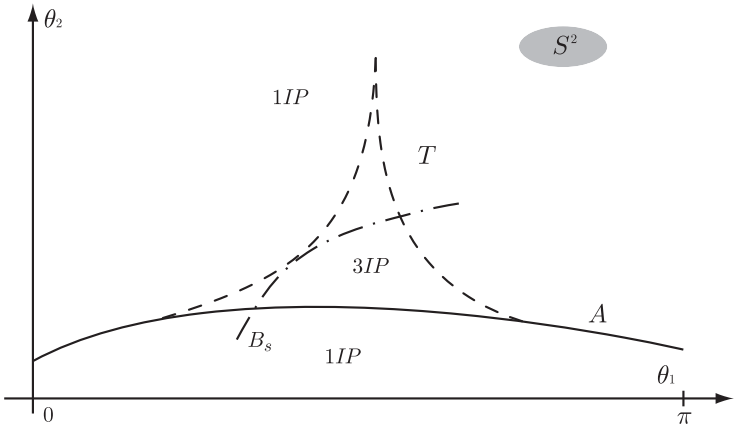

Figure 1.4: Standard diagram and a B_s curve for the 1PI case

The standard diagram for a constant pitch helix is shown in Fig. 1.4. The A-curve is drawn as a solid line, and the $T-$curve is drawn as a dashed line. Each point in the diagram corresponds to a plane through x. The two curves divide S^2 into several regions. Within each of them all planes have the same number of intersection points (IPs) with $C_{PI}(x)$. For example, the curves in Fig. 1.4 divide S^2 into two regions - with one IP and three IPs, respectively (1IP and 3IP regions, for short). Recall that the boundaries $\theta_1 = 0$ and

$\theta_1 = \pi$ of the rectangle $[0, \pi] \times [0, \pi]$ are glued together with a twist according to (1.22). For instance, the upper right corner in Fig. 1.4 is glued to the lower left corner. See [Kat06] for more details on such diagrams.

We also need the so-called B_s-curves (see [Kat06]). For a fixed $s \in I_{PI}(x)$, B_s is the great circle formed by the vectors orthogonal to $x - y(s)$. Let us illustrate the connection between the B_s curves and filtering lines on the detector plane. As follows from the results in [Kat03], given $s \in I_{PI}(x)$, the filtering lines are determined by finding the discontinuities of the function

$$\phi(s, x, \theta) := \operatorname{sgn}(\alpha \cdot \dot{y}(s)) n(s, x, \alpha), \ \alpha = \alpha(s, \theta) \in \beta^{\perp}(s, x). \tag{1.23}$$

Note that $\alpha(s, \theta), \theta \in [0, 2\pi]$, moves precisely along the curve B_s. Here θ is the polar angle in the plane $\beta^{\perp}(s, x)$. Since n is normalized, n can be discontinuous when the number of IPs changes, i.e. when B_s intersects either the A- or the T-curve. A discontinuity of n across the T-curve (as well as the discontinuity of $\operatorname{sgn}(\alpha \cdot \dot{y}(s))$) is not harmful to the FBP structure of the algorithm, because it happens across the plane tangent to the helix, and there are sufficiently many $x \in U$ that share the same tangent plane. On the other hand, a discontinuity of n across the A-curve ruins the FBP structure, because such a discontinuity occurs across the plane containing the PI line of x, and there is only a one-dimensional set of $x \in U_{PI}$ which share that PI line. Hence the requirement is that n be continuous across the A-curve for all B_s-curves, $s \in I_{PI}(x)$.

Consider the original inversion formula (1.6). It can be easily shown that it is based on the following weight function. If α is in the 1IP region, $n(s_1, x, \alpha) = 1$. Here $y(s_1)$ denotes

the only IP of $\Pi(x,\alpha)$ and $C_{PI}(x)$. If α is in the 3IP region, there are three IPs $s_1 < s_2 < s_3$, and their weights are $n(s_1,x,\alpha) = n(s_3,x,\alpha) = 0$, $n(s_2,x,\alpha) = 1$. Fix any $s \in I_{PI}(x)$ and consider what happens when the curves B_s and A intersect. When B_s enters the 3IP region, two new IPs appear. Since they are located near the boundary of $I_{PI}(x)$, the IPs are given weight zero. Hence the IP s has the same weight $n(s,x,\alpha) = 1$ on either side of the A-curve, thereby guaranteeing the continuity of n across A.

As was already mentioned, any $x \in U$ has a diagram of the type shown in Fig. 1.4 if the helix satisfies the convexity condition. If the condition is violated, then the diagrams change as well. Clearly, only the following two critical changes are possible: (a) Self-intersection of the T-curve, and (b) Intersection of the T- and A-curves in the interior of T.

Self-intersections of the T-curve. Self-intersections of the T-curve are not harmful to the FBP structure of the algorithm. All additional discontinuities of $n(s,x,\alpha)$ that arise because of the self-intersection still occur only when B_s intersects the T-curve. Thus, they can be taken into account by introducing additional filtering lines in the original 1PI algorithm. Clearly, these filtering lines are tangent to the projected helix. Two such violations are illustrated in Fig. 1.5.

Intersection of the T- and A-curves. An intersection of the $T-$ and A-curves is potentially harmful to the FBP structure of the algorithm. If they do intersect, there can be several different 3IP regions in a neighborhood of the A-curve. In this case a B_s curve could go from one 3IP region to another across the A-curve (see [Kat06]). Consequently, we would

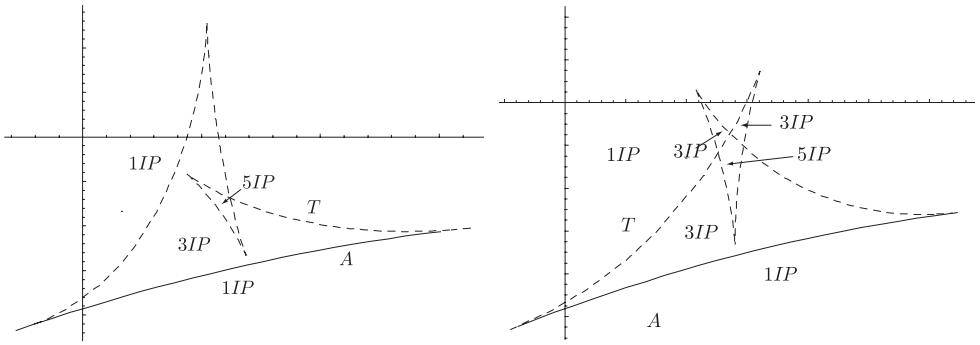

Figure 1.5: Formation of new regions away from the A-curve

not be able to use the idea in which two extreme IPs are given weight zero (see the second paragraph following (1.23)). Thus, we need to find the subset $U' \subset U_{PI}$ such that for any $x \in U'$ the T- and A-curves do not intersect. This is done by finding the *b*oundary of U'.

Pick a point $x_0 \in U_{PI} \backslash U'$ (i.e. such that the T- and A-curves of x_0 intersect) and $x_1 \in U'$. Connect x_0 and x_1 by a continuous path in U_{PI}. Since diagrams depend continuously on x, there exists a point x^* on the path such that the diagram of x^* exhibits one of the following *c*ritical properties:

1. The $T-$curve touches the A-curve at an interior point of the PI interval;

2. The order of tangency at one of the endpoints of the PI interval is increased.

Hence the boundary of U' is a subset of points, whose diagrams exibit critical properties (1) or (2). In what follows we derive the conditions that describe the two critical cases and determine the boundary of U' using these conditions.

1.4 Analysis of critical cases

This section focuses upon deriving conditions that describe the critical cases stated at the end of section 1.3. We also verify that U' depends continuously on the perturbation of the source trajectory. Then we present the results of calculating the boundary of U' for a chosen $\mu(s)$.

Pick $x \in U_{PI}$, so x admits a unique PI line. Let its endpoints be $y(s_b)$ and $y(s_t)$. The first critical case occurs when the T-curve touches the A-curve at an interior point of $I_{PI}(x)$. Hence there exists a value $s_0 \in I_{PI}(x)$ such that $\alpha(s_0)$ (cf. (1.20)) is orthogonal to the PI line:

$$\alpha(s_0) \cdot (y(s_t) - y(s_b)) = [y(s_t) - y(s_b), x - y(s_0), \dot{y}(s_0)] = 0, \tag{1.24}$$

i.e. the plane passing through $y(s_0)$ and the PI line touches the curve at s_0 (or, equivalently, contains $\dot{y}(s_0)$). The tangency at s_0 implies that $\dot{\alpha}(s_0)$ is parallel to $\alpha(s_0) \times (y(s_t) - y(s_b))$, i.e.

$$\begin{aligned} &\dot{\alpha}(s_0) \times \{\alpha(s_0) \times (y(s_t) - y(s_b))\} \\ &= \alpha(s_0) \{\dot{\alpha}(s_0) \cdot (y(s_t) - y(s_b))\} - (y(s_t) - y(s_b))(\alpha(s_0) \cdot \dot{\alpha}(s_0)) \\ &= \alpha(s_0) \{\dot{\alpha}(s_0) \cdot (y(s_t) - y(s_b))\} = 0, \end{aligned} \tag{1.25}$$

where in the last step we used that $\dot{\alpha}(s_0) \perp \alpha(s_0)$. Thus, differentiating (1.20) and setting $s = s_0$, we get after simple transformations

$$\dot{\alpha}(s_0) \cdot (y(s_t) - y(s_b)) = [y(s_t) - y(s_b), x - y(s_0), \ddot{y}(s_0)] = 0, \tag{1.26}$$

where we have used that equality (1.24) holds at s_0.

Thus, the tangency of T- and A-curves implies that there exists a point $y(s_0), s_0 \in [s_b, s_t]$, such that the plane containing the PI line and passing through $y(s_0)$ contains $\dot{y}(s_0)$ and $\ddot{y}(s_0)$. Equivalently, $\Pi_{osc}(s_0)$ intersects the helix at two points $y(s_b)$ and $y(s_t)$, where $s_0 - 2\pi < s_b < s_0 < s_t < s_0 + 2\pi$.

Arguing in a similar fashion we establish that the increased order of tangency of the T- and A-curves at an endpoint of the PI interval implies that the osculating plane at one of the endpoints intersects the helix at the other endpoint.

In summary, the boundary of U' is a subset of the surface formed by chords $H(l, r)$ which have one of the following properties:

(1) There exists $c \in [l, r]$ such that $\Pi_{osc}(c)$ intersects the helix at $y(l)$ and $y(r)$,

(2) $\Pi_{osc}(l)$ intersects the helix at $y(r)$,

(3) $\Pi_{osc}(r)$ intersects the helix at $y(l)$.

For reasons that become clear in section 1.5, we relax the restrictions on c in (1) and replace condition (1) with

(1') There exists $c \in (r - 2\pi, l + 2\pi)$, such that $\Pi_{osc}(c)$ intersects the helix at $y(l)$ and $y(r)$.

Here we also need to add another restriction on the severity of the violation, namely the chords connecting intersection points of osculating planes with the helix should not be very far apart. More precisely,

Condition 2. *For all c, if $\Pi_{osc}(c)$ intersects C at $y(l)$ and $y(r)$, then $|l-c|<\pi$, $|r-c|<\pi$ and $|l-r|<\pi$.*

Note that it follows from the subsequent discussion that if the violation of the convexity condition is small, such chords are indeed localized near the source trajectory.

Region where the osculating planes intersect the helix. Fix s and suppose that $\Pi_{osc}(s)$ intersects the helix at $q=q(s,\varepsilon)$, $0<|q-s|<2\pi$. Then:

$$D(s,q,\varepsilon)=[y(q)-y(s),\dot{y}(s),\ddot{y}(s)]=\begin{vmatrix}\cos q-\cos s & \sin q-\sin s & \psi(q,\varepsilon)-\psi(s,\varepsilon)\\ -\sin s & \cos s & \dot{\psi}(s,\varepsilon)\\ -\cos s & -\sin s & \ddot{\psi}(s,\varepsilon)\end{vmatrix}=0. \tag{1.27}$$

We will show that (1.27) admits two solutions q_l and q_r, which depend continuously on μ. By the implicit function theorem,

$$q'_\varepsilon(s,\varepsilon)=-\frac{D'_\varepsilon(s,q,\varepsilon)}{D'_q(s,q,\varepsilon)}. \tag{1.28}$$

Since $D(s,q,\varepsilon)$ is linear in ε, the derivative $D'_\varepsilon(s,q,\varepsilon)$ is well-defined. Furthermore,

$$D'_q(s,q,\varepsilon)\big|_{q=q(s,\varepsilon),\varepsilon=0}=\begin{vmatrix}-\sin q & \cos q & \dot{\psi}(q)\\ -\sin s & \cos s & \dot{\psi}(s)\\ -\cos s & -\sin s & \ddot{\psi}(s)\end{vmatrix}. \tag{1.29}$$

We shall use the results of [KBH04] on the convexity of projected helices. According to [KBH04], the curvature of the projected helix at the point q projected onto $DP(s)$ is given up to a positive factor by $\Phi(q,s)$ (see (1.15) for the definition).

Here we need to add the final constraint on the severity of the violation, namely:

Condition 3. *Γ_- and Γ_+ do not intersect for any s.*

Now we consider the following three cases.

Case I: $s \in (A, B)$. Using (1.15) and (1.8), we see that the sign of the curvature of the projected helix behaves as shown in table 1.1, where s_l, s_r are some values which satisfy $s_l < A < B < s_r$. Using table 1.1 and condition 3, we see that in this case the projections of Γ_- and Γ_+ look like those shown in Fig. 1.6.

Table 1.1: Sign of curvature of the projected helix, the case $s \in (A, B)$.

$(s - 2\pi, s_l)$	(s_l, s)	(s, s_r)	$(s_r, s + 2\pi)$
$-$	$+$	$-$	$+$

Thus, for a fixed $s \in (A, B)$ and a sufficiently small $\varepsilon > 0$ there exist two solutions of (1.27). We denote the two solutions by q_l and q_r. From Fig. 1.6, $q_l < s_l < A < s < B < s_r < q_r$.

By construction, $D(s, q, 0) = 0$ for $0 < |q - s| < 2\pi$ if and only if the projected helix intersects the common asymptote L_0. Using an argument analogous to the one in section 1.2, the fact that $q_l < s_l$ and $s_r < q_r$, and table 1.1, we conclude that $D'_q(s, q_l, 0) > 0$, $D'_q(s, q_r, 0) > 0$.

Case II: $s > B$. Again, the sign of the curvature of the projected helix can be summarized as in table 1.2, where $s_l < A < s_r < B < s$. Using table 1.2 and condition 3, we see that in this case the projections of Γ_- and Γ_+ look like those shown in Fig. 1.7.

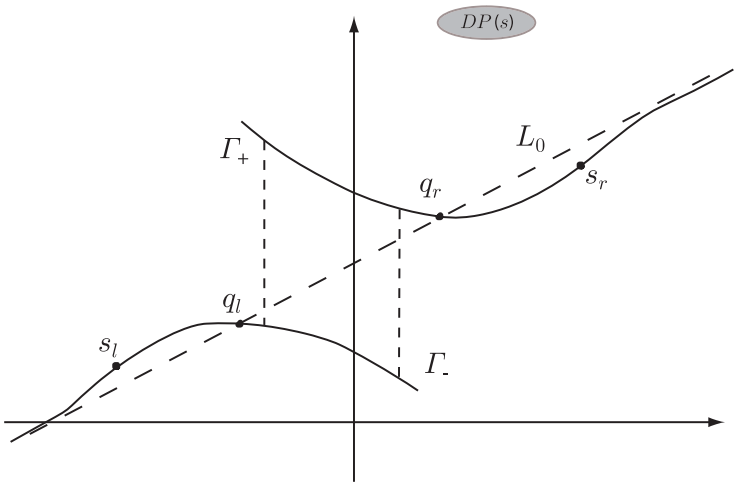

Figure 1.6: Projection of the helix onto $DP(s)$ for $s \in (A, B)$

Table 1.2: Sign of curvature of the projected helix, the case $s > B$.

$(s - 2\pi, s_l)$	(s_l, s_r)	(s_r, s)	$(s, s + 2\pi)$
$-$	$+$	$-$	$+$

Thus, if s is sufficiently close to B, there are two solutions of the equation $D(s, q, \varepsilon) = 0$ as well, and they satisfy $q_l < s_l < q_r < s_r < s$ (see Fig. 1.7).

Similarly to case I, one establishes that $D'_q(s, q_l, 0) > 0$, $D'_q(s, q_r, 0) < 0$, so these derivatives are nonzero as long as $q_r \neq q_l$ and $q_r, q_l \neq s$.

Case III: The case $s < A$ is analogous to Case II.

Our argument shows that the chords, which satisfy properties 1', 2 and 3 stated prior to Condition 2 depend continuously on μ as long as $q_l \neq q_r$. If $q_l \to q_r$, then the two critical chords $H(s, q_l)$ and $H(s, q_r)$ collide and disappear. So the boundary of U' depends continuously on μ.

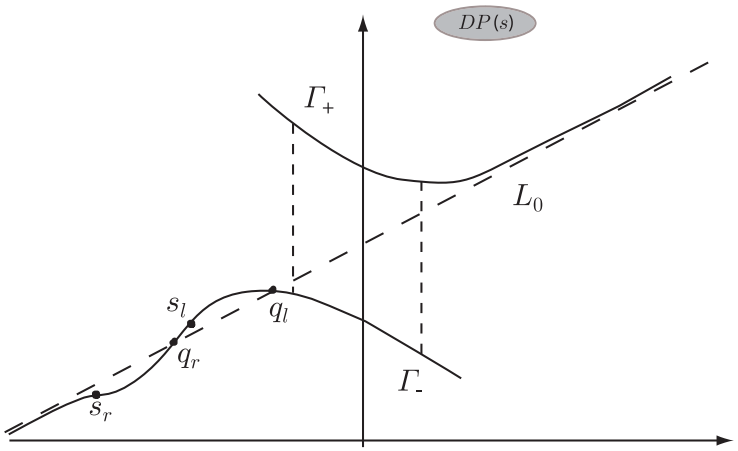

Figure 1.7: Projection of the helix onto $DP(s)$ for $s > B$

Summarizing the results of sections 1.2 and 1.4, we *d*efine U_0 as the largest cylinder strictly inside U' and centered around the x_3-axis. The cross-section of the boundaries of U' and U_{PI} corresponding to the plane $x_3 = \psi(0)$ in the case of μ given by (1.34) is shown in Fig. 1.8. For that particular μ the cylinder of radius 0.4 can be taken as U_0. The next section focuses upon deriving backprojection coefficients for exact reconstruction inside U_0 and proving that the resulting algorithm is detector-driven.

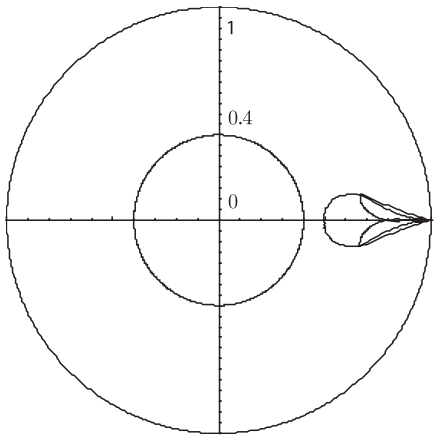

Figure 1.8: The boundaries derived in sections 1.2 and 1.4 for the chosen source trajectory

1.5 Backprojection coefficients

In this section we modify the original reconstruction algorithm to make it applicable to image reconstruction inside the set U_0, which was defined at the end of section 1.4. An important property of the algorithm is that it is detector-driven. More precisely, for any $x \in U_0$ and $s \in I_{PI}(x)$, the filtering lines are determined only by the projection of x on $DP(s)$. In particular, one never needs to determine the PI line through x.

Let $\hat{x}(s)$ denote the projection of x onto $DP(s)$. If the value of s is irrelevant at the moment, we write simply $\hat{x}$. Similarly, whenever a geometrical object (e.g., a point, vector, PI line, etc.) is projected onto $DP(s)$, the corresponding projection is denoted by hat.

Finding filtering lines on the detector plane passing through $\hat{x}$ amounts to finding lines passing through $\hat{x}$ that are tangent to $\Gamma_- \cup \Gamma_+$ inside $I_{PI}(x)$. In the original algorithm the latter requirement can be easily enforced without knowing $I_{PI}(x)$ by imposing the following conditions:

FL1. A filtering line through $\hat{x}$ is tangent to Γ_+, and the point of tangency is to the right of $\hat{x}$;

FL2. A filtering line through $\hat{x}$ is tangent to Γ_-, and the point of tangency is to the left of $\hat{x}$.

Proposition 1.5.2 below shows that these conditions also hold for $x \in U_0$. This ensures that the resulting algorithm is detector-driven.

Let us now state some propositions that are needed in the subsequent discussion. The proofs of the propositions are in Appendix.

Proposition 1.5.1. *For any $x \in U_0$ and $s \in I_{PI}(x)$, $\hat{L}_{PI}(x)$ intersects $\Gamma_- \cup \Gamma_+$ only twice.*

Proposition 1.5.2. *For $x \in U_0$, if a filtering line satisfies conditions FL1, FL2, the point of tangency is inside $I_{PI}(x)$.*

Proposition 1.5.3. *For $x \in U_0$, the slope of $\hat{L}_{PI}(x)$ on $DP(s)$ is always greater than the slope of any filtering line through $\hat{x}(s)$, which satisfies conditions FL1, FL2.*

We now proceed to derive the backprojection coefficients. In what follows we fix $x \in U_0$ and derive the filtering lines and corresponding backprojection coefficients so that the modified inversion algorithm is theoretically exact. Clearly, we need to consider the following two cases:

1. Almost any plane through x has one or three intersections with $C_{PI}(x)$;

2. Almost any plane through x has one, three, or five intersections with $C_{PI}(x)$.

Let us denote one of the IPs by $y(s_0)$ and consider $DP(s_0)$. Consider the first case. Using Propositions 1.5.1 and 1.5.3, it can be easily seen from the two projections shown in Figures 1.6 and 1.7 that there exists a unique value $s_{tan} \in I_{PI}(x)$ such that the plane containing x, $y(s_0)$ and $y(s_{tan})$ touches $C_{PI}(x)$ at $y(s_{tan})$. By assumption, almost all planes have only one or three IPs with $C_{PI}(x)$, so there is no 5IP region on the diagram of x (i.e. the $T-$curve has no self-intersections). Thus, the diagram of x corresponds to the standard

case. Consequently, the original algorithm applies without any modifications: the filtering lines and corresponding backprojection coefficients are the same.

Consider now the second case. Suppose $y(s_0)$ belongs to a 5IP-plane of x. Again, using Propositions 1.5.1 and 1.5.3, and taking into account the possible shapes of the projected helix shown in Figures 1.6 and 1.7, we see that there exist three values $s_{tan,j}$ such that the plane through x, $y(s)$ and $y(s_{tan,j})$ is tangent to the projection of C at $y(s_{tan,j})$, $j = 1, 2, 3$, and conditions FL1, FL2 hold. It follows from Proposition 1.5.2 that all points of tangency necessarily belong to $C_{PI}(x)$ as long as $x \in U_0$.

Define the following vectors:

$$e_j(s, \beta) := \frac{(\beta \times \dot{y}(s_{tan,j})) \times \beta}{|(\beta \times \dot{y}(s_{tan,j})) \times \beta|}, \tag{1.30}$$

where $\beta = \beta(s, x)$. Recall that the projection of $e_j(s, x)$ on $DP(s)$ is denoted by $\hat{e}_j(s, x)$. We also denote $L(s, x, \alpha) := \Pi(x, \alpha) \cap DP(s)$ and write $L(x, \alpha)$ when s is fixed and irrelevant for the current discussion. For convenience we always assume that $\hat{e}_j(s, x)$ *h*ave been arranged in the order of decreasing slopes. Taking Proposition 1.5.3 into account, we conclude that the following properties hold:

1. $\Pi(x, \alpha)$ has three IPs with $C_{PI}(x)$ if and only if $L(x, \alpha)$ is between $\hat{L}_{PI}(x)$ and $\hat{e}_1(s, x)$ or between $\hat{e}_2(s, x)$ and $\hat{e}_3(s, x)$;

2. $\Pi(x, \alpha)$ has five IPs with $C_{PI}(x)$ if and only if $L(x, \alpha)$ is between $\hat{e}_1(s, x)$ and $\hat{e}_2(s, x)$.

Since all 5IP planes intersect $DP(s)$ in the wedge between $\hat{e}_1(s, x)$ and $\hat{e}_2(s, x)$, this wedge collapses as x leaves U_{5IP}. Thus, we refer to the other two filtering lines, $\hat{e}_0(s, x)$ and

$\hat{e}_3(s,x)$, as the 'standard' filtering lines. The same argument as in [Kat02b] can be used to show that if $\Pi(x,\alpha)$ is a 3IP plane, then the standard filtering lines and backprojection coefficients $c_0 = c_3 = 1/2$ guarantee that $\Pi(x,\alpha)$ gets the total weight 1.

Now suppose $\Pi(x,\alpha)$ is a 5IP plane. We will see that the use of only the 'standard' filtering lines and backprojection coefficients leads to a total weight $\neq 1$ being assigned to $\Pi(x,\alpha)$. To fix the problem, we add two more filtering lines on the detector plane so that these two filtering lines assign weight 1 to all 5IP planes and 0 to all 1IP and 3IP planes. Then a scaling of the obtained weights by a certain constant corrects the total weighting in the 5IP region without violating the weights in the 1IP and 3IP regions. Moreover, the assigned weights ensure the continuity of the filtering step as x leaves U_{5IP}.

As follows from the projections in Figures 1.6 and 1.7, we need to consider the following three cases depending on the position of $\dot{y}(s)$ relative to $\hat{e}_j(s_0,x)$, $j = 1,2,3$, on $DP(s)$. We denote $\hat{e}_0(s,x) := \dot{y}(s)$ for convenience, and let c_j be the backprojection coefficient assigned to the filtering line along the vector $\hat{e}_j(s,x)$, $j = 0,1,2,3$.

1. $\dot{y}(s)$ is above $\hat{e}_1(s,x)$. Then $c_0 = 0, c_1 = 1/2$, and $c_2 = -1/2$.

2. $\dot{y}(s)$ is below $\hat{e}_2(s,x)$. Then $c_0 = 0, c_1 = -1/2$, and $c_2 = 1/2$.

3. $\dot{y}(s)$ is between $\hat{e}_1(s,x)$ and $\hat{e}_2(s,x)$. Then $c_0 = 1$ and $c_1 = c_2 = 1/2$.

In all three cases $c_3 = 0$. One easily sees that in each of the three cases

$$\sum_{j=0}^{2} c_j \mathrm{sgn}(e_j(s,x)\cdot\alpha)\mathrm{sgn}(\dot{y}(s)\cdot\alpha) = \begin{cases} 1, & \text{if } L(x,\alpha) \text{ lies between } \hat{e}_1(s,x) \text{ and } \hat{e}_2(s,x), \\ 0, & \text{otherwise.} \end{cases} \tag{1.31}$$

Next we consider the weights that 5IP planes through x get if **o**nly the standard filtering lines $\hat{e}_0(s_0), \hat{e}_3(s_0,x)$, and coefficients $c_0 = c_3 = 1/2$ are used. Suppose $\Pi(x,\alpha)$ intersects $C_{PI}(x)$ at five points $\{y(s_k)\}_{k=1}^5$. We need to calculate

$$\frac{1}{2}\sum_{k=1}^{5} \mathrm{sgn}(e_0(s_k,x)\cdot\alpha)\cdot\mathrm{sgn}(\dot{y}(s_k)\cdot\alpha) + \frac{1}{2}\sum_{k=1}^{5} \mathrm{sgn}(e_3(s_k,x)\cdot\alpha)\cdot\mathrm{sgn}(\dot{y}(s_k)\cdot\alpha). \tag{1.32}$$

The first sum is easy to calculate, since all the expressions under the sum are equal to 1:

$$\frac{1}{2}\sum_{k=1}^{5} \mathrm{sgn}(e_0(s_k,x)\cdot\alpha)\cdot\mathrm{sgn}(\dot{y}(s_k)\cdot\alpha) = 5/2. \tag{1.33}$$

The expression under the second sum equals 1 when $\dot{y}(s_k)$ is below $L(x,\alpha)$ on $DP(s_k)$, and equals -1 when $\dot{y}(s_k)$ is above $L(x,\alpha)$ on $DP(s_k)$. It can be easily seen from the projections of the helix that for $x \in U_0$ and for any 5IP plane $\Pi(x,\alpha)$ intersecting $C_{PI}(x)$, the projection of $\dot{y}(s_k)$ is above $L(x,\alpha)$ on $DP(s_0), DP(s_2), DP(s_4)$ and below $L(x,\alpha)$ on $DP(s_1), DP(s_3)$. Thus the second sum always equals $-1/2$. Adding up the contributions from $\dot{y}(s_k)$ and $\hat{e}_3(s_k,x)$, we obtain $-1/2 + 5/2 = 2$.

Consequently, the coefficients c_0, c_1, c_2 defined in (1)–(3) above should be scaled by the factor $-1/5$ to compensate for the extra weight of 1 that $\Pi(x,\alpha)$ gets when it is in the 5IP region and added to the 'standard' coefficients.

Thus, we have obtained the following algorithm. For $\hat{x} \in DP(s)$, in addition to $\hat{e}_0(s,x)$, find all tangent filtering lines on $DP(s)$ through $\hat{x}$ subject to conditions FL1, FL2.

1. If there is only one tangent filtering line determined by $\hat{e}_1(s,x)$, set $c_0 = c_1 = 1/2$;

2. If three tangent filtering lines pass through $\hat{x}$, sort them in decreasing order of slopes. Let $\hat{e}_1(s,x)$, $\hat{e}_2(s,x)$, $\hat{e}_3(s,x)$ be the corresponding vectors. Then the backprojection coefficients are assigned according to the following algorithm:

   (a) if $\dot{y}(s)$ is above $\hat{e}_1(s,x)$, then $c_0 = 1/2, c_1 = -1/10, c_2 = 1/10, c_3 = 1/2$;

   (b) if $\dot{y}(s)$ is below $\hat{e}_2(s,x)$, then $c_0 = 1/2, c_1 = 1/10, c_2 = -1/10, c_3 = 1/2$;

   (c) if $\dot{y}(s)$ is between $\hat{e}_1(s,x)$ and $\hat{e}_2(s,x)$, then $c_0 = 3/10, c_1 = 1/10, c_2 = 1/10, c_3 = 1/2$.

The inversion formula is then given by (1.6), where we use $M(s) = 1$ or 3 depending on how many filtering lines pass through $\hat{x}$, and the corresponding backprojection coefficients are determined according to the above scheme. Case (a) is illustrated in Fig. 1.9. One can also see that the algorithm continuously transforms into the standard algorithm, since as x moves out of U_{5IP}, the two additional lines tend to each other and their backprojection coefficients cancel. Similarly, the algorithm is continuous as $\dot{y}(s)$ moves across $\hat{e}_1(s,x)$ and $\hat{e}_2(s,x)$.

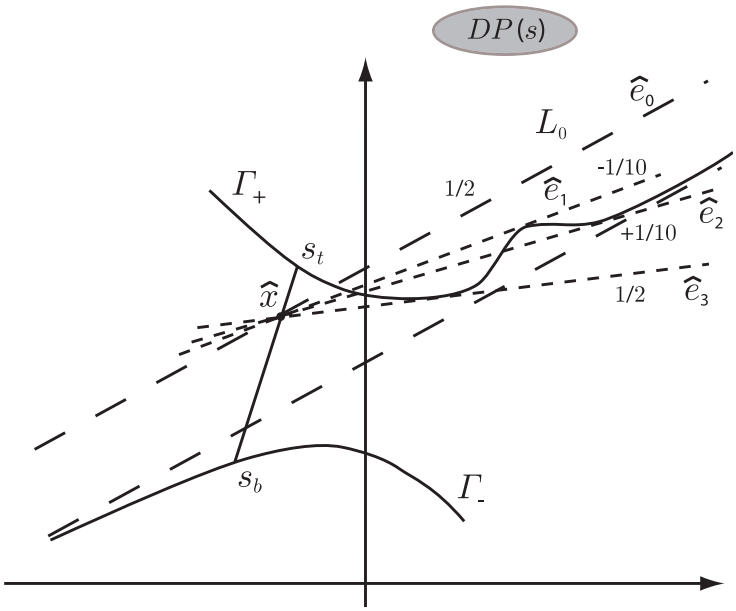

Figure 1.9: Filtering lines on the detector plane and the corresponding backprojection coefficients

1.6 Numerical experiments

Numerical experiments were conducted using flat detector geometry. Parameters of our reconstructions are summarized in Table 1.3. The algorithm was implemented in the native coordinates as described in [NPH03]. The following sample $\mu(s)$ was chosen for the simulations (see Fig. 1.10):

$$\mu(s) = \begin{cases} 8.333, & s < -0.7 \\ 37.5, & -0.7 < s \leq -0.4 \\ -10.750, & -0.4 \leq s \leq 0.4 \\ 37.5, & 0.4 \leq s < 0.7 \\ 8.333, & s \geq 0.7 \end{cases} \tag{1.34}$$

Table 1.3: Simulation parameters

Parameter	Value	Units
Source to rotation axis distance	600	mm
Number of detector columns	1201	
Detector pixel size at isocenter	0.5×0.5	mm^2
Number of detector rows	181	
Views per rotation	2000	

The numbers in the definition of μ are not round, because the perturbation of a constant speed helix had to be compactly supported and, therefore, satisfy the conditions stated below (1.12).

As one sees from the graph of $\dot{\psi}(s)$ used for simulations (see Fig. 1.10), the source trajectory undergoes a perturbation such that the maximum table speed reaches approximately 1.35 of the steady-state speed. Note that despite the three restrictions imposed on U_0, a cylinder with radius 40% of the source to rotation axis distance and centered about the x_3-axis can be reconstructed exactly.

In the first experiment we reconstructed the clock phantom (see e.g., [KBH04]). The background cylinder was at 0 HU, the spheres were at 1000 HU, and the air at -1000 HU. The reconstruction result is shown in Fig. 1.11.

As was already mentioned in section 1.1, a violation of the convexity condition may lead to the appearance of the set $U_{5IP} \subset U$. The reason why such a set appears is that the

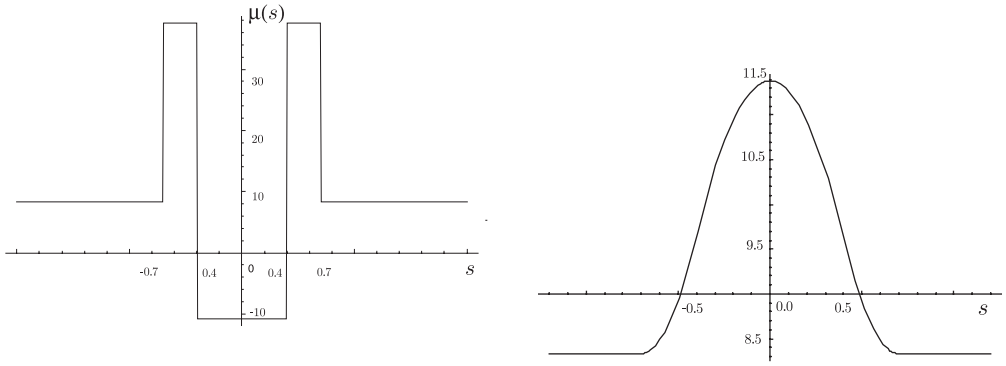

Figure 1.10: Graph of the $\mu(s)$ chosen for the simulations (left panel) and the corresponding $\dot{\psi}(s)$ (right panel)

T-curve of $x \in U_{5IP}$ self-intersects (cf. section 1.3). Figure 1.5 shows two types of diagrams for points in U_{5IP}. One can show that inside U_0 only three types of diagrams are possible: the standard one in Figure 1.4 and the two in Figure 1.5. In fact, $U_{5IP} \cap U_0 \neq \varnothing$, so artifacts may occur even inside U_0 if the violation of the convexity condition is ignored. To illustrate the artifact we simulated a flat disk, which has a sharp z-transition in the set $U_{5IP} \cap U_0$. The parameters of the disk are: center (191, 0, 5), half-axes (35, 35, 5). The disk was at 1000 HU, and the background at 0 HU.

Since the standard algorithm assumes that there is always one tangent filtering line for all $\hat{x}$ inside the Tam window (in addition to $\hat{e}_0(s, x)$), one needs to make an assumption on which tangent line the algorithm chooses. We performed reconstructions using the following three algorithms:

1. the standard algorithm choosing $\hat{e}_1(s, x)$ as the filtering line (Fig. 1.12, first image from the left)

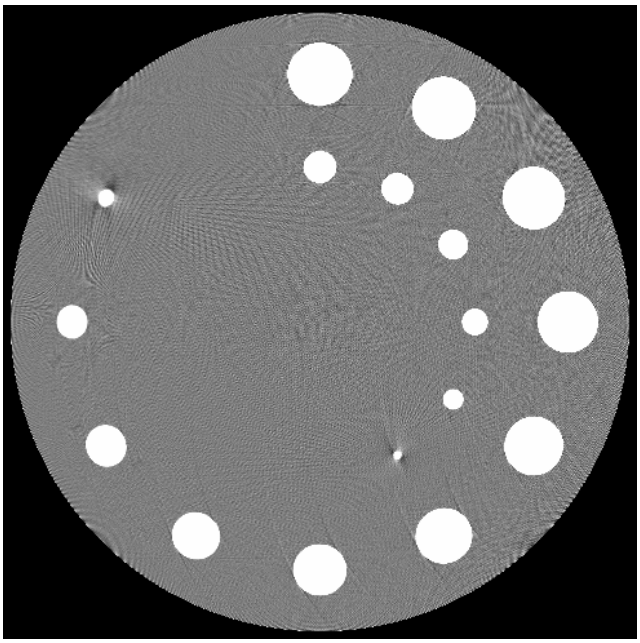

Figure 1.11: Reconstruction of the clock phantom: slice $z = 0$, WL=0 HU, WW=100 HU

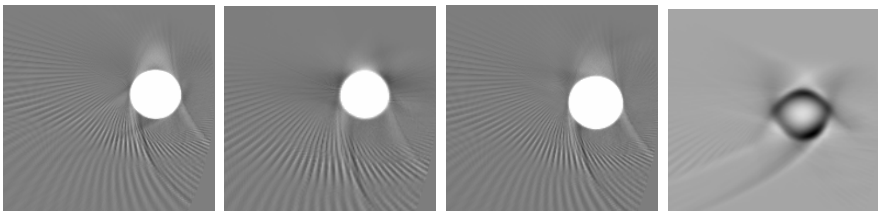

Figure 1.12: Reconstructions of the flat disk phantom, WL=0 HU, WW=60 HU

2. the standard algorithm choosing $\hat{e}_3(s, x)$ as the filtering line (Fig. 1.12, second image from the left)

3. the exact algorithm (Fig. 1.12, third image from the left).

The right image in Fig. 1.12 shows the difference between the first and third images from the left.

As is seen from the results, the original algorithm given by (1.6) is not very sensitive to medium perturbations of the source trajectory. If one completely ignores the violation and uses simply the first tangent filtering line in addition to $\hat{e}_0(s,x)$, this results in a high-frequency artifact (see the left and right panels in Fig. 1.12). Choosing $\hat{e}_3(s,x)$ as the filtering direction instead of $\hat{e}_1(s,x)$ eliminates the high-frequency artifact, but introduces some darkening to the left and right of the disk (see the second image from the left in Fig. 1.12). In all cases the artifacts were not too prominent, especially when compared with the artifact that is caused by the cut-off at the boundary of the Tam window (the streaks extending down from the disk). Comparing with the reconstruction results presented in [NPH03] and [YW04], we see that the improved 1PI algorithm of [Kat02a] provides better image quality than the original algorithm (1.6). We have generalized the results obtained here to the improved 1PI algorithm of [Kat02a]. A paper describing this generalization is currently in preparation – [KK].

A GENERAL CLASS OF CURVES

This chapter is organized as follows. In Section 2.1 we define PI-lines for general curves, describe precisely the class of curves considered in this chapter, and study properties of their PI-segments. In Section 2.2 we find the set U where PI-lines are guaranteed to be unique. The result is based on the notions of maximal and minimal PI-lines. These critical PI-lines can be viewed as a generalization of the axial direction for regular helices. Also we find the special planes, such that the stereographic projection of C onto these planes has very useful properties. In Section 2.3 we study more properties of the PI-segments of C. Then the inversion formula is given. Finally, the results of numerical experiments are presented in Section 2.4.

2.1 PI lines and their properties

The objective of this section is to define PI lines for a general class of smooth curves and study their properties. Let C be a smooth curve:

$$I := [a, b] \ni s \to y(s) \in \mathbb{R}^3, \ |\dot{y}(s)| \neq 0. \tag{2.1}$$

Here and below the dot above a variable denotes differentiation with respect to s. Define the functions

$$\Phi(s, s_0) := [y(s) - y(s_0), \dot{y}(s), \ddot{y}(s)], \ Q(s, s_0) := [y(s) - y(s_0), \dot{y}(s_0), \dot{y}(s)], \tag{2.2}$$

where $[e_1, e_2, e_3] := e_1 \cdot (e_2 \times e_3)$ denotes the scalar triple product of three vectors. If C is a helix, then Φ and Q are precisely the functions that have been introduced under the same names in [KBH04]. Similarly to [KBH04], it turns out later that Φ is intimately related to the convexity of the projection of C onto a detector plane (cf. (2.35) below), and Q is related to the uniqueness of PI-lines (cf. Definitions 2.1.1, 2.1.2, equation (2.23), and the proof of Proposition 2.2.2). Given any $s_0, s_1 \in I$, $H(s_0, s_1)$ denotes the line segment with the endpoints $y(s_0), y(s_1) \in C$.

Definition 2.1.1. *Pick two points $y(s_0), y(s_1) \in C$, $s_0 < s_1$. The line segment $H(s_0, s_1)$ is called the PI-segment if $Q(s, q) \neq 0$ for any $s, q \in [s_0, s_1]$, $s \neq q$.*

Definition 2.1.2. *Pick two points $y(s_0), y(s_1) \in C$, $s_0 < s_1$. The line segment $H(s_0, s_1)$ is called the maximal PI-segment if $Q(s_0, s_1) = 0$, but $Q(s, q) \neq 0$ for any $s, q \in (s_0, s_1)$, $s \neq q$.*

If C is a helix, definition 2.1.1 gives the usual PI-segments $H(s, q), 0 < q - s < 2\pi$, and definition 2.1.2 gives the maximal PI-segments $H(s, s + 2\pi)$.

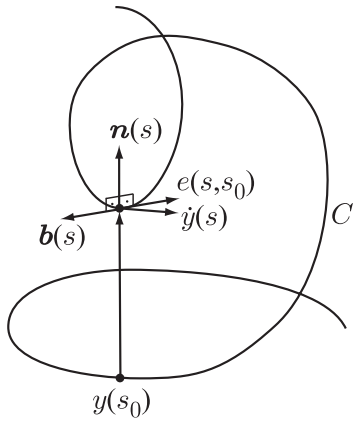

Figure 2.1: Critical case

Next we discuss how a smooth curve bends. Consider two points: $y(s_0), y(s) \in C$. Assume $y(s_0)$ is fixed, and $y(s)$ moves along C. The line segment joining $y(s_0)$ and $y(s)$ rotates about the instantaneous axis $e(s, s_0) = (y(s) - y(s_0)) \times \dot{y}(s)/|(y(s) - y(s_0)) \times \dot{y}(s)|$. The point $y(s)$ rotates also about the instantaneous axis, which is obtained by finding the circle of curvature of C at $y(s)$ (also known as the osculating circle). The corresponding axis of rotation is $\mathbf{b}(s)$, i.e. the binormal vector. If $s \to s_0$, then $e(s, s_0) \to \mathbf{b}(s)$. Thus, the difference in directions of the two vectors can measure how much the curve bends between the two points. The maximum possible "bent" occurs when the two axes point in the opposite directions: $e(s, s_0) = -\mathbf{b}(s)$ (see Figure 2.1).

Now we can formulate the main assumptions on the curve C.

C1. C is smooth, and the curvature and torsion of C are positive;

C2. C does not self-intersect within any PI-segment (or a maximal PI-segment) of C;

C3. Given any PI-segment (or a maximal PI-segment) $H(s_0, s)$ of C, there is no line tangent to C at $y(s_1)$ and intersecting C at $y(s_2)$ with $s_1, s_2 \in [s_0, s]$, $s_1 \neq s_2$;

C4. C does not bend too much, i.e. given any PI-segment (or a maximal PI-segment) $H(s_0, s)$ of C, one has $e(s_1, s_2) \neq -\mathbf{b}(s_2)$ for any $s_1, s_2 \in [s_0, s]$, $s_1 \neq s_2$.

If a curve satisfies conditions C1–C4, then its PI-segments have a number of nice properties.

Proposition 2.1.1. *Let C be a curve, which satisfies conditions C1–C4, and let $H(s_0, s_1)$ be its (possibly maximal) PI-segment. Then for any $s, q \in [s_0, s_1]$ one has: $\Phi(s, q) > 0$ if $s > q$ and $\Phi(s, q) < 0$ if $s < q$.*

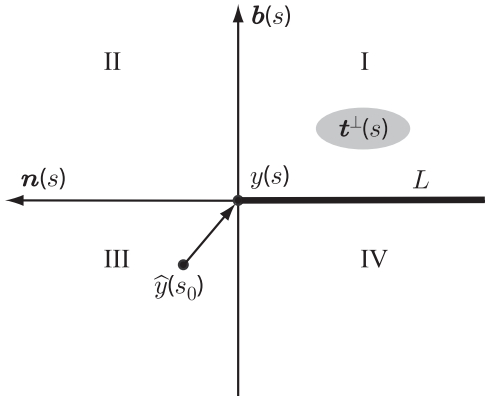

Figure 2.2: Projection of $y(s_0)$ onto the plane through $y(s)$ with normal vector $\dot{y}(s)$

Proof. By shrinking the PI-line if necessary, the proposition follows if we show that $\Phi(s, s_0) \neq 0$ for any $s \in (s_0, s_1]$ and $\Phi(s, s_1) \neq 0$ for any $s \in [s_0, s_1)$. We prove only the first statement, because the proof of the second one is analogous.

Let us assume that the parameterization of $y(s)$ is natural, i.e. $|\dot{y}(s)| \equiv 1$. For convenience, recall the Frenet-Serret formulas:

$$\begin{bmatrix} \dot{\mathbf{t}} \\ \dot{\mathbf{n}} \\ \dot{\mathbf{b}} \end{bmatrix} = \begin{bmatrix} 0 & \kappa & 0 \\ -\kappa & 0 & \tau \\ 0 & -\tau & 0 \end{bmatrix} \begin{bmatrix} \mathbf{t} \\ \mathbf{n} \\ \mathbf{b} \end{bmatrix}, \tag{2.3}$$

where $\mathbf{t}(s), \mathbf{n}(s), \mathbf{b}(s)$ are the unit tangent, normal and binormal vectors, respectively, $\kappa(s)$ is the curvature and $\tau(s)$ is the torsion of the source trajectory. Using (2.3), we get

$$\begin{aligned}\Phi(s, s_0) = [y(s) - y(s_0), \dot{y}(s), \ddot{y}(s)] =& \kappa(s)[y(s) - y(s_0), \mathbf{t}(s), \mathbf{n}(s)] \\ =& \kappa(s)\mathbf{b}(s) \cdot (y(s) - y(s_0)).\end{aligned} \tag{2.4}$$

Since we are interested in the sign of $\Phi(s, s_0)$ and $\kappa(s) > 0$, we determine the sign of

$$\begin{aligned}\mathbf{b}(s) \cdot (y(s) - y(s_0)) &= \int_{s_0}^{s} (\mathbf{b}(t) \cdot (y(t) - y(s_0)))'_t \, dt \\ &= -\int_{s_0}^{s} \tau(t)\mathbf{n}(t) \cdot (y(t) - y(s_0))dt.\end{aligned} \tag{2.5}$$

Let $\mathbf{t}^{\perp}(s)$ denote the plane passing through $y(s)$ and perpendicular to $\mathbf{t}(s)$. We assume that $\mathbf{n}(s)$ and $\mathbf{b}(s)$ are the coordinate axes on the plane, and $y(s)$ is the origin (see Figure 2.2).

Let $\Pi_{osc}(s)$ denote the osculating plane of C at $y(s)$. Recall that $\Pi_{osc}(s)$ contains $y(s)$ and is parallel to $\dot{y}(s)$ and $\ddot{y}(s)$. If $y(s_0)$ projects onto the ray $L := y(s) - \lambda\mathbf{n}(s), \lambda > 0$, then $y(s_0)$ belongs to $\Pi_{osc}(s)$. Moreover, the two rotation axes: one, determined by rotation of $y(s)$ around $y(s_0)$, and the other, $\mathbf{b}(s)$ - determined by rotation of $y(s)$ relative to the intrinsic center of rotation, are parallel and point in the opposite directions. This is prohibited by the assumption that the curve does not bend too much, so $y(s_0)$ never projects onto L.

Let $\hat{y}(s_0)$ denote the projection of $y(s_0)$ onto $\mathbf{t}^{\perp}(s)$. The Taylor series expansions shows that $\tau > 0$ and $\kappa > 0$ imply

$$\mathbf{n}(t) \cdot (y(s) - y(s_0)) < 0, \ \mathbf{b}(s) \cdot (y(s) - y(s_0)) > 0, \tag{2.6}$$

for $s - s_0 > 0$ small enough. Hence, initially $\hat{y}(s_0)$ is located in the third quadrant (see Figure 2.2). Suppose now s increases. If $\hat{y}(s_0)$ appears in the third quadrant, then $\mathbf{n}(t) \cdot$

$(y(t) - y(s_0)) < 0$. So $\mathbf{b}(s) \cdot (y(s) - y(s_0))$ increases, $\hat{y}(s_0)$ moves down and does not cross the $\mathbf{n}$-axis. If $\hat{y}(s_0)$ appears in the fourth quadrant, then $\mathbf{n}(t) \cdot (y(t) - y(s_0)) > 0$ and $\mathbf{b}(s) \cdot (y(s) - y(s_0))$ decreases. This implies that in the fourth quadrant $\hat{y}(s_0)$ moves up. However, our assumption precludes $\hat{y}(s_0)$ from crossing L. Consequently, $\hat{y}(s_0)$ never crosses the $\mathbf{n}$-axis and $\Phi(s, s_0) > 0$ for any $s \in (s_0, s_1]$. □

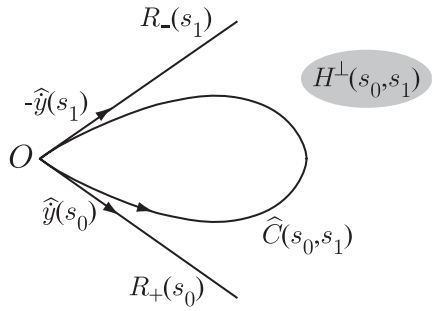

Figure 2.3: Illustration of the containment property: orthogonal projection onto $H^\perp(s_0, s_1)$

Let $H(s_0, s_1)$ be a PI-segment (possibly maximal), and $C(s_0, s_1)$ the corresponding curve segment. Project $C(s_0, s_1)$, $\dot{y}(s_0)$, and $\dot{y}(s_1)$ orthogonally onto a plane perpendicular to $H(s_0, s_1)$. Such a plane is denoted $H^\perp(s_0, s_1)$. The corresponding projections are denoted $\hat{C}(s_0, s_1)$, $\hat{\dot{y}}(s_0)$, and $\hat{\dot{y}}(s_1)$, respectively (see Figure 2.3). Let O be the projection of $H(s_0, s_1)$. The vectors $\hat{\dot{y}}(s_0)$ and $\hat{\dot{y}}(s_1)$ determine two rays:

$$\begin{aligned} R_+(s_0) :=& \{x \in H(s_0, s_1)^\perp : x = O + \lambda \hat{\dot{y}}(s_0), \lambda \geq 0\}, \\ R_-(s_0) :=& \{x \in H(s_0, s_1)^\perp : x = O + \lambda(-\hat{\dot{y}}(s_1)), \lambda \geq 0\}. \end{aligned} \tag{2.7}$$

Proposition 2.1.2. *Let C be a curve, which satisfies conditions C1–C4. If $H(s_0, s_1)$ is a (possibly maximal) PI-segment of C, then one has:*

1. *$\hat{C}(s_0, s_1)$ is contained inside the wedge with vertex O and formed by the rays $R_+(s_0)$ and $R_-(s_1)$;*

2. *$\hat{C}(s_0, s_1)$ is smooth and no line through O is tangent to $\hat{C}(s_0, s_1)$ at an interior point;*

3. *If $H(s_0, s_1)$ is not maximal, the angle between $R_+(s_0)$ and $R_-(s_1)$ is less than π. If $H(s_0, s_1)$ is maximal, the angle between the rays equals π;*

4. *No line through O intersects the interior of $\hat{C}(s_0, s_1)$ at more than one point.*

The property of C described in statement (1) of the proposition is important for us, so it will be given the name containment property. In other words, statement (1) says that PI-segments of curves, which satisfy conditions C1–C4, have the containment property.

Proof. To show that $\hat{C}(s_0, s_1)$ is contained inside the wedge, we first consider $\hat{C}(s_0, s)$, where $s = s_0 + \epsilon$ for some $0 < \epsilon \ll 1$. As is easily seen, containment follows from the two inequalities:

$$\begin{aligned} &[y(t) - y(s_0), y(s_1) - y(s_0), \dot{y}(s_0)] > 0 \ \forall t \in (s_0, s_1), \\ &[y(t) - y(s_0), y(s_1) - y(s_0), \dot{y}(s_1)] > 0 \ \forall t \in (s_0, s_1). \end{aligned} \tag{2.8}$$

To prove the first inequality introduce the function

$$\Psi(s_1, t) := \left[\frac{y(t) - y(s_0) - \dot{y}(s_0)(t - s_0)}{(t - s_0)^2}, \frac{y(s_1) - y(s_0) - \dot{y}(s_0)(s_1 - s_0)}{(s_1 - s_0)^2}, \dot{y}(s_0) \right]. \tag{2.9}$$

By using the Taylor series expansions we see that $\Psi(s_1, t)$ is smooth and bounded on compact sets. Notice also that

$$\Psi(s_1, s_1) = 0, \ \Psi'_t(s_1, t) < \infty. \tag{2.10}$$

Hence $\Psi(s_1,t)/(s_1-t)$ is bounded as well, which implies

$$\begin{aligned}&[y(t)-y(s_0),y(s_1)-y(s_0),\dot{y}(s_0)]\\&\quad=\frac{(t-s_0)^2(s_1-s_0)^2(s_1-t)}{12}([\dot{y}(s_0),\ddot{y}(s_0),\dddot{y}(s_0)]+o(1))>0,\end{aligned}\tag{2.11}$$

where $o(1)\to 0$ as $s_1\to s_0$. The second inequality in (2.8) can be proven for small $s_1-s_0>0$ in a similar fashion.

Suppose now s_1-s_0 is not necessarily small. Note that $\hat{C}(s_0,s_1)$ is tangent to the rays $R_+(s_0)$ and $R_-(s_1)$ at the point O of order precisely one. Consider, for example, the ray $R_+(s_0)$. To determine the order of tangency we need to find the asymptotics of the first expression in (2.8) as $t\to s_0$, with s_0 and s_1 fixed. We have:

$$\begin{aligned}&[y(t)-y(s_0),y(s_1)-y(s_0),\dot{y}(s_0)]\\&\quad=[\ddot{y}(s_0),y(s_1)-y(s_0),\dot{y}(s_0)]\frac{(t-s_0)^2}{2}+O\left((t-s_0)^3\right)\\&\quad=-\Phi(s_0,s_1)\frac{(t-s_0)^2}{2}+O\left((t-s_0)^3\right).\end{aligned}\tag{2.12}$$

Similarly,

$$[y(t)-y(s_0),y(s_1)-y(s_0),\dot{y}(s_1)]=\Phi(s_1,s_0)\frac{(t-s_1)^2}{2}+O\left((t-s_1)^3\right),\ t\to s_1.\tag{2.13}$$

By Proposition 2.1.1, $\Phi(s_0,s_1)<0$, $\Phi(s_1,s_0)>0$, and the desired assertion follows.

Suppose $C(s_0,s_1)$ does not have the containment property. Assume, for example, that the first inequality in (2.8) is violated. A violation of the other inequality can be considered analogously. From (2.12) and Proposition 2.1.1, the inequality holds for some $t>s_0$, where $t-s_0$ is sufficiently small. Thus there exists $t\in(s_0,s_1)$ such that

$$[y(t)-y(s_0),y(s_1)-y(s_0),\dot{y}(s_0)]=0.\tag{2.14}$$

Equation (2.14) defines t as a function of s_1. Differentiating (2.14) with respect to s_1 gives:

$$\frac{dt}{ds_1} = -\frac{[y(t) - y(s_0), \dot{y}(s_1), \dot{y}(s_0)]}{[\dot{y}(t), y(s_1) - y(s_0), \dot{y}(s_0)]}. \tag{2.15}$$

The denominator in (2.15) does not vanish. Otherwise, from the linear independence of $\dot{y}(s_0)$ and $y(s_1) - y(s_0)$ (property C3) and (2.14) we get $Q(t, s_0) = [y(t) - y(s_0), \dot{y}(s_0), \dot{y}(t)] = 0$. Since $H(s_0, s_1)$ is a PI-line, this is a contradiction. Hence we can consider the function $t(s)$ for some $s \leq s_1$ using that $Q(t, s_0) \neq 0$ for $t \in (s_0, s_1)$. As s decreases from s_1 towards s_0, one of the following must happen:

a) $s, t \to s^* \neq s_0$. Replacing s_1 with s, and t - with $t(s)$ in (2.14) gives $Q(s^*, s_0) = [y(s^*) - y(s_0), \dot{y}(s_0), \dot{y}(s^*)] = 0$, which contradicts the assumption that $H(s_0, s_1)$ is a PI-line.

b) $t \to s_0$, $s \to s^* > s_0$. From (2.14), $\Phi(s_0, s^*) = [y(s_0) - y(s^*), \dot{y}(s_0), \ddot{y}(s_0)] = 0$, which contradicts Proposition 2.1.1.

Note that $s, t \not\to s_0$ because of (2.11). Thus the containment property is established.

To prove the second statement we argue by contradiction. Suppose there exists $t \in (s_0, s_1)$, where either $\hat{C}(s_0, s_1)$ is non-smooth or where the line through O and $\hat{y}(t)$ is tangent to $\hat{C}(s_0, s_1)$. Here $\hat{y}(t)$ is the projection of $y(t)$ onto $H^{\perp}(s_0, s_1)$. In both cases

$$[y(s_1) - y(s_0), \dot{y}(t), y(t) - y(s_0)] = 0. \tag{2.16}$$

Just as in the proof of statement (1), (2.16) defines t as a function of s_1. Differentiating (2.16) with respect to s_1 gives:

$$\frac{dt}{ds_1} = -\frac{[\dot{y}(s_1), \dot{y}(t), y(t) - y(s_0)]}{[y(s_1) - y(s_0), \ddot{y}(t), y(t) - y(s_0)]}. \tag{2.17}$$

The denominator in (2.17) does not vanish. Otherwise, together with (2.16) this gives $\Phi(t, s_0) = [y(t) - y(s_0), \dot{y}(t), \ddot{y}(t)] = 0$, which contradicts Proposition 2.1.1. Here we have used the fact that $y(s_1) - y(s_0)$ and $y(t) - y(s_0)$ are not parallel (cf. (2.8)). Hence we can consider the function $t(s)$ for some $s \leq s_1$ using that $\Phi(t, s_0) \neq 0$ for $t \in (s_0, s_1]$. As s decreases from s_1 towards s_0, one of the following must happen:

a) $s, t \to s^* \neq s_0$. Replacing s_1 with s and t with $t(s)$ in (2.16) gives $[y(s^*) - y(s_0), \dot{y}(s^*), \ddot{y}(s^*)] = 0$, which contradicts Proposition 2.1.1.

b) $t \to s_0$, $s \to s^* > s_0$. Then (2.16) implies $[y(s^*) - y(s_0), \dot{y}(s_0), \ddot{y}(s_0)] = 0$, which is again a contradiction.

c) $s, t \to s_0$. Now (2.16) implies $[\dot{y}(s_0), \ddot{y}(s_0), \dddot{y}(s_0)] = 0$, i.e. $\tau(s_0) = 0$. This contradicts the assumption $\tau(s_0) > 0$.

Our argument proves that (2.16) does not happen, so statement (2) is established.

To prove statement (3), first consider $H(s_0, q)$ for $q - s_0 > 0$ sufficiently small. As follows from statements (1) and (2), $\hat{C}(s_0, q)$ is contained between the rays $R_+(s_0)$ and $R_-(q)$, which are close to each other. As q increases towards s_1, the two rays cannot collapse into one. Because of the containment, $\hat{C}(s_0, q)$ is always located between the rays. So if the two rays

collapse into one for some $q > s_0$, then $C(s_0, q)$ is a planar curve, which contradicts the assumption $\tau > 0$. Hence $Q(s_0, s_1) = 0$ if and only if $R_+(s_0)$ and $R_-(s_1)$ point in the opposite directions (see Figure 2.5).

Statements (1)–(3) imply that (i) whenever a line through O intersects $\hat{C}(s_0, s_1)$, then all the intersection points (IPs) are on one side of O; and (ii) neither $R_+(s_0)$ nor $R_-(s_1)$ intersects the interior of $\hat{C}(s_0, s_1)$. By (i) we can replace "line" with "ray" in statement (4). Suppose there is a ray γ with vertex at O, which intersects $\hat{C}(s_0, s_1)$ at two interior points. Clearly, by rotating γ around O towards either $R_+(s_0)$ or $R_-(s_1)$ we can make the two IPs collide. As soon as the IPs collide, we get a ray tangent to $\hat{C}(s_0, s_1)$ at an interior point, which contradicts statement (2). □

Corollary 2.1.1. *No plane intersects $C(s_0, s_1)$ at more than three points.*

Proof. Suppose there is a plane Π that has at least four IPs with $C(s_0, s_1)$: $s_0 \leq t_1 < t_2 < t_3 < t_4 \leq s_1$. Consider $C(t_1, t_4)$ and project it onto the plane perpendicular to $H(t_1, t_4)$ (as was done in the proof of Proposition 2.1.2). As before, let O denote the projection of $H(t_1, t_4)$. The projection of Π gives the line through O, which intersects $\hat{C}(t_1, t_4)$ at least at two points, which contradicts statement (3) of Proposition 2.1.2. □

Corollary 2.1.2. *Pick any $x \in H(s_0, s_1)$ and $s \in (s_0, s_1)$. Consider a plane Π rotating around the axis $\beta(s, x)$. The number of IPs of Π and $C(s_0, s_1)$ changes from one to three when Π passes through $H(s_0, s_1)$.*

Proof. Consider the critical case when Π contains $H(s_0, s_1)$. As follows from Proposition 2.1.2, the vectors $\dot{y}(s_0)$ and $-\dot{y}(s_1)$ point into the opposite half-planes relative to Π. Hence, a small rotation of Π around $\beta(s, x)$ in one direction gives 1IP, and in the opposite direction - 3IPs. See Section 4 in [Kat06] for more details. □

2.2 Establishing uniqueness of PI lines

To establish uniqueness of PI lines, we generalize the standard argument from helices [KND00, KL03, KBH04] to general curves.

Fix $x \in U$. For each $s \in I$, fix a vector $N(s)$, $|N(s)| \equiv 1$ (a specific $N(s)$ will be chosen later). Define the functions $q(s)$ and $\lambda(s)$ so that $q(s) > s$, $H(s, q(s))$ is a PI-segment, $0 < \lambda(s) < 1$, and the point

$$x(s) := y(s) + \lambda(s)(y(q(s)) - y(s)) \in H(s, q(s)) \tag{2.18}$$

has the property

$$x(s) - x \parallel N(s). \tag{2.19}$$

We assume that the functions $q(s)$ and $\lambda(s)$ with the required properties exist. Later (see (2.27) and the proof of Proposition 2.2.2) we find U such that for any $x \in U$ the functions $q(s)$ and $\lambda(s)$ do exist.

Condition (2.19) means that the parallel projection of $x(s)$ onto the plane through x with normal vector $N(s)$ coincides with x. Note that the vector-valued function $N(s)$ is

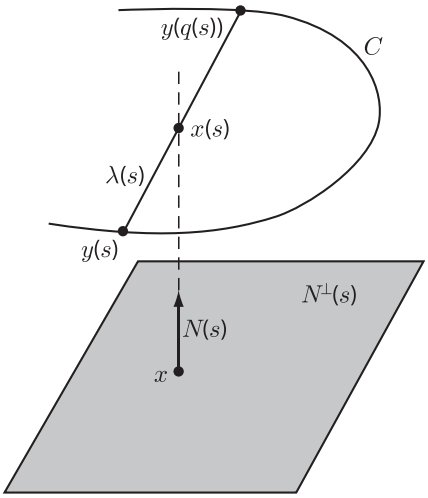

Figure 2.4: Parallel projection onto the plane $N^{\perp}(s)$ through x

determined independently of $q(s)$ and $\lambda(s)$. A similar idea is used in proving the uniqueness of PI lines for the standard helix, the difference being that the vector $N(s)$ is constant and directed along the axis of the helix.

Figure 2.4 illustrates the setup: the functions $q(s)$ and $\lambda(s)$ are defined in such a way as to ensure that the parallel projection of $x(s)$ onto the plane through x with normal $N(s)$ always coincides with x. Denote $\Delta y(s) := y(q(s)) - y(s)$. Thus,

$$\varepsilon(s) := N(s) \cdot \{(y(s) + \lambda(s)\Delta y(s)) - x\} \tag{2.20}$$

is the signed distance from $y(s) + \lambda(s)\Delta y(s)$ to x, i.e. $\varepsilon(s) = 0$ if and only if the chord $H(s, q(s))$ passes through x. We are interested in calculating $\varepsilon'(s)$.

Combining (2.18)–(2.20) gives

$$y(s) + \lambda(s)(y(q(s)) - y(s)) = x + \varepsilon(s)N(s). \tag{2.21}$$

Differentiate (2.21) with respect to s:

$$\dot{y}(s) + \lambda'(s)\Delta y(s) + \lambda(\dot{y}(q(s))q'(s) - \dot{y}(s)) = \varepsilon'(s)N(s) + \varepsilon(s)\dot{N}(s). \tag{2.22}$$

Computing the dot product of (2.22) with $\Delta y(s) \times \dot{y}(q)$ on both sides gives the expression:

$$\begin{aligned} &\varepsilon'(s) = A(s) + \varepsilon(s)B(s), \\ &A(s) := -(1-\lambda(s))\frac{Q(s,q(s))}{[N(s), \Delta y(s), \dot{y}(q(s))]},\ B(s) := -\frac{[\dot{N}(s), \Delta y(s), \dot{y}(q(s))]}{[N(s), \Delta y(s), \dot{y}(q(s))]}, \end{aligned} \tag{2.23}$$

where we have used (2.2).

The goal is to obtain the uniqueness of PI lines. We start by choosing a vector $N(s)$ in such a way as to ensure that the denominator in (2.23) is never zero as long as $H(s, q(s))$ is a PI line. Denote the supremum (respectively, infimum) of all q such that $H(s, q)$ is a PI line by $q_{max}(s)$ (respectively, $q_{min}(s)$). Since $I = [a, b]$ is a compact interval, $q_{max}(s)$ and $q_{min}(s)$ are well-defined.

Our assumptions imply that the function $q_{max}(s)$ is continuous on (a, b). If $q_{max}(s) = b$ for some $s \in (a, b)$, then $q_{max}(t) \equiv b$ for all $t \in (s, b)$. If $q_{max}(s) < b$ for some $s \in (a, b)$, then

$$Q(q_{max}(s), s) = [y(q_{max}(s)) - y(s), \dot{y}(s), \dot{y}(q_{max}(s))] = 0. \tag{2.24}$$

Differentiating (2.24) with respect to s gives

$$q'_{max}(s) = -\frac{[y(q_{max}(s)) - y(s), \ddot{y}(s), \dot{y}(q_{max}(s))]}{[y(q_{max}(s)) - y(s), \dot{y}(s), \ddot{y}(q_{max}(s))]}. \tag{2.25}$$

By assumption C2, $y(q_{max}(s)) - y(s)$ and $\dot{y}(s)$ are never parallel. Hence, if the denominator in (2.25) is zero, together with (2.24) this implies

$$[y(q_{max}(s)) - y(s), \dot{y}(q_{max}(s)), \ddot{y}(q_{max}(s))] = 0,$$

which contradicts Proposition 2.1.1. Our argument implies that $q'_{max}(s)$ can have at most one point of discontinuity. If the discontinuity exists, then $q'_{max}(s) = 0$ to the right of it, and $q'_{max}(s)$ is given by (2.25) to the left of it.

In a similar fashion we obtain that $q_{min}(s)$ is continuous, and $q'_{min}(s)$ is piece-wise continuous on (a, b). Define

$$N_{max}(s) := \frac{y(q_{max}(s)) - y(s)}{|y(q_{max}(s)) - y(s)|},\ N_{min}(s) := \frac{y(q_{min}(s)) - y(s)}{|y(q_{min}(s)) - y(s)|},\ s \in (a, b). \tag{2.26}$$

Thus, $N_{max}(s)$ (resp., $N_{min}(s)$) is the unit vector along $H(s, q_{max}(s))$ (resp., $H(q_{min}(s), s)$).

Proposition 2.2.1. *Pick any $t \in (s, q_{max}(s))$. One has $[y(t) - y(s), \dot{y}(t), N_{max}(s)] \neq 0$, and the curve segments $C(s, t)$ and $C(t, q_{max}(s))$ are located on the opposite sides of the plane containing $H(s, q_{max}(s))$ and $y(t)$. Similarly, pick any $t \in (q_{min}(s), s)$. One has $[y(t) - y(s), \dot{y}(t), N_{min}(s)] \neq 0$, and the curve segments $C(t, s)$ and $C(q_{min}(s), t)$ are located on the opposite sides of the plane containing $H(q_{min}(s), s)$ and $y(t)$.*

Proof. We only prove the statements concerning $q_{max}(s)$. The other half of the proposition is completely analogous.

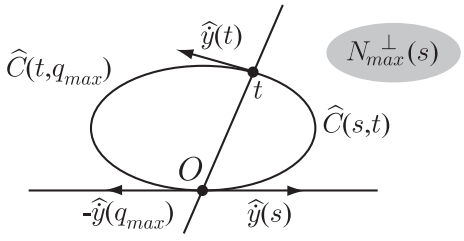

Figure 2.5: Projection onto the plane $N_{max}(s)^{\perp}$

The assertion $[y(t) - y(s), \dot{y}(t), N_{max}(s)] \neq 0$ follows immediately from statement (2) of Proposition 2.1.2 (see also its proof). This proposition also implies that any line, which contains O and passes between the rays $R_+(s_0)$ and $R_-(s_1)$, divides $\hat{C}(s, q_{max})$ into two segments located in the opposite half-planes (see Figure 2.5). This means that the curve segments $C(s,t)$ and $C(t, q_{max}(s))$ are located on the opposite sides of the plane containing $H(s, q_{max}(s))$ and $y(t)$. □

Next we determine the region where PI-lines, if exist, are unique. Even though the curve C is well-behaved locally, very little can be said about the global behavior of C. So we choose a "local" piece of C: $I_0 := [a_0, b_0] \subset (a, b)$. The word local is made precise later. For each $s \in I_0$ consider the curve $\hat{C}(s, q_{max})$ in the plane $N^{\perp}_{max}(s)$. By construction, $\hat{C}(s, q_{max})$ is closed. Let $Cyl_{max}(s)$ be the infinite open cylinder with axis $N_{max}(s)$, whose base is the interior of $\hat{C}(s, q_{max})$. In the same fashion we define the cylinders $Cyl_{min}(s)$ using $\hat{C}(q_{min}, s)$ and $N_{min}(s)$. Define U as the intersection of all such open cylinders:

$$U := \cap_{s \in I_0} \left(Cyl_{min}(s) \cap Cyl_{max}(s) \right). \tag{2.27}$$

If the curve turns too much, U can be empty. As an example, imagine a "slinky" toy. Locally it looks like a section of a helix. However if the slinky twists too much and the interval I_0 is sufficiently large, there can be no x that belongs to all the cylinders. We assume that a sufficiently "local" piece of C is taken, so $U \neq \varnothing$. Note that in the case of helix all cylinders $Cyl_{min}(s)$ and $Cyl_{max}(s)$ are identical, so (2.27) gives the usual domain inside the helix.

Proposition 2.2.2. *Pick $x \in U$. If x admits a PI-line, it is unique in the sense that there is no other PI-line with an endpoint inside I_0.*

Proof. Choose $N(s) := N_{max}(s)$ in (2.19). Since $x \in U$, x projects along $N(s)$ into the interior of $\hat{C}(s, q_{max})$ for any $s \in I_0$. Hence the functions $q(s)$, $\lambda(s)$, and the map $s \to x(s)$ (cf. (2.18), (2.19)) are well-defined on I_0. By Proposition 2.2.1, $[\Delta y(s), \dot{y}(q(s)), N(s)] \neq 0$ for any $s \in I_0$, i.e. $\varepsilon'(s)$ is smooth on I_0. By construction, $H(s, q(s))$ are PI-segments, so $Q(s, q(s)) \neq 0$ on I_0. Similarly, $\lambda(s) < 1$ on I_0.

Our argument implies that $A(s)$ (cf. (2.23)) is bounded away from zero and of constant sign on I_0. Consider now $B(s)$ (cf. (2.23)). As we already know, the denominator is bounded away from zero. Differentiating (2.26) gives

$$\begin{aligned} \dot{N}_{max}(s) =& \frac{1}{|y(q_{max}(s)) - y(s)|} \\ & \times \left\{ [\dot{y}(q_{max}(s)) q'_{max}(s) - \dot{y}(s)] - N \left(N \cdot [\dot{y}(q_{max}(s)) q'_{max}(s) - \dot{y}(s)] \right) \right\}. \end{aligned} \tag{2.28}$$

By assumption C1, C has no self-intersections, so $|y(q_{max}) - y(s)|$ is bounded away from zero. From (2.25) and the subsequent discussion, it follows that $q'_{max}(s)$ is bounded away from zero. Hence, $\dot{N}_{max}(s)$ is bounded, and $B(s)$ is bounded as well.

From the properties of $A(s)$ and $B(s)$ we get that $\varepsilon(s)$ cannot have more than one root on I_0. This follows immediately from the fact that the signs of $\varepsilon'(s)$ and $A(s)$ in a neighborhood of any s where $\varepsilon(s) = 0$ are the same. Hence x cannot have more than one PI-segment with $s_b(x) \in I_0$.

Choosing $N(s) := N_{min}(s)$ in (2.19) and repeating the same argument gives that x cannot have more than one PI-segment with $s_t(x) \in I_0$. □

2.3 Reconstruction algorithm

In order to derive an inversion formula we need to study the curve C some more.

Proposition 2.3.1. *Let $H(s_0, s_1)$ be a (possibly maximal) PI-segment of C. Then $\hat{C}(s_0, s_1)$ has everywhere non-vanishing curvature.*

Proof. Recall that $\hat{C}(s_0, s_1)$ is smooth by Proposition 2.1.2. Pick any $t \in (s_0, s_1)$ and suppose the curvature vanishes there. This implies

$$[y(s_1) - y(s_0), \dot{y}(t), \ddot{y}(t)] = 0, \tag{2.29}$$

which means that $y(s_1) - y(s_0)$ is parallel to $\Pi_{osc}(t)$. Since $\tau(t) \neq 0$, $C(t-\epsilon, t)$ and $C(t, t+\epsilon)$ are on the opposite sides of $\Pi_{osc}(t)$ for some $\epsilon > 0$. By Proposition 2.1.1, $\Pi_{osc}(t)$ does not intersect $C(s_0, s_1)$ at any point other than $y(t)$. Hence $C(s_0, t)$ and $C(t, s_1)$ are on the opposite sides of $\Pi_{osc}(t)$. In particular, the line segment $H(s_0, s_1)$ intersects $\Pi_{osc}(t)$, which contradicts (2.29). If $t = s_0$ or $t = s_1$, the desired assertion follows immediately from Proposition 2.1.1. □

Corollary 2.3.1. *Let $H(s_0, s_1)$ be a (possibly maximal) PI-segment of C. For any $x \in H(s_0, s_1)$ and $t \in (s_0, s_1)$, the vectors $\dot{y}(t)$ and $x - y(t)$ are not collinear.*

Proof. By Proposition 2.1.1, $\hat{C}(s_0, q_{max}(s_0))$ is strictly convex. $x \in H(s_0, s_1)$ implies that x projects into the domain bounded by $\hat{C}(s_0, q_{max}(s_0))$. Thus $\dot{y}(t)$ and $x - y(t)$ are not collinear. □

Proposition 2.3.2. *Let $H(s_0, s_1)$ be a (possibly maximal) PI-segment of C. For any $x \in H(s_0, s_1)$ there exists the unique $s^*(x)$ such that $x \in \Pi_{osc}(s^*(x))$.*

Proof. As follows from the proof of Proposition 2.3.1, $\Pi_{osc}(t)$ intersects $H(s_0, s_1)$ for any $t \in [s_0, s_1]$. Hence we can write

$$y(s_0) + \lambda(t)(y(s_1) - y(s_0)) = y(t) + a(t)\dot{y}(t) + b(t)\ddot{y}(t) \tag{2.30}$$

for some scalar functions λ, a, and b. Differentiate (2.30) with respect to t, multiply the resulting equation by $\dot{y}(t) \times \ddot{y}(t)$ and solve for λ':

$$\lambda'(t) = b(t)\frac{[\dot{y}(t), \ddot{y}(t), \dddot{y}(t)]}{[y(s_1) - y(s_0), \dot{y}(t), \ddot{y}(t)]}. \tag{2.31}$$

Since the torsion of C is non-zero, the numerator in (2.31) does not vanish. From the proof of Proposition 2.3.1, the denominator in (2.31) is non-zero. By Corollary 2.3.1, $b(t) \neq 0, t \in (s_0, s_1)$. Hence $\lambda(t)$ is a smooth monotone function on $[s_0, s_1]$. Obviously, $\Pi_{osc}(s_0)$ (resp., $\Pi_{osc}(s_1)$) intersects $H(s_0, s_1)$ at $y(s_0)$ (resp., $y(s_1)$). Thus $\lambda(s_0) = 0$, $\lambda(s_1) = 1$, and the proposition is proven. □

Due to the containment property (statement (1) of Proposition 2.1.2), the curve $C(s, q_{max}(s))$ (resp., $C(s, q_{min}(s))$) is on one side of the plane passing through $y(s)$ and parallel to $\dot{y}(s)$ and $N_{max}(s)$ (resp., $N_{min}(s)$). This makes it very convenient to project $C(s, q_{max}(s))$ (resp.,

$C(s, q_{min}(s)))$ onto a plane parallel to $\dot{y}(s)$ and $N_{max}(s)$ (resp., $N_{min}(s)$). The corresponding projections turn out to be smooth. Let $DP_+(s)$ (resp., $DP_-(s)$) denote a plane not passing through $y(s)$ and parallel to $\dot{y}(s)$ and $N_{max}(s)$ (resp., $N_{min}(s)$). The stereographic projection of $C(s, q_{max}(s))$ onto $DP_+(s)$ is denoted Γ_+, while the stereographic projection of $C(q_{min}(s), s)$ onto $DP_-(s)$ is denoted Γ_-.

Proposition 2.3.3. *Γ_+ and Γ_- are smooth and have nonvanishing curvature at every point.*

Proof. We only consider Γ_+. The statement about Γ_- is proven analogously. Suppose, for simplicity, that the origin is at $y(s)$, and the equation of $DP_+(s)$ is $x_3 = 1$. Thus, x_1 and x_2 are the coordinates on $DP_+(s)$. Let $x_1(t)$ and $x_2(t)$ be the coordinates of the projection of $y(t), t \in (s, q_{max}(s))$, onto $DP_+(s)$. Then

$$x_1(t) = \frac{y_1(t)}{y_3(t)},\ x_2(t) = \frac{y_2(t)}{y_3(t)}. \tag{2.32}$$

As is well-known,

$$\kappa(t) = \frac{\dot{x}_1^2}{(\dot{x}_1^2 + \dot{x}_2^2)^{3/2}} \left(\frac{\dot{x}_2}{\dot{x}_1}\right)'. \tag{2.33}$$

Differentiating (2.32) gives

$$\begin{aligned} \left(\frac{\dot{x}_2}{\dot{x}_1}\right)' &= \left(\frac{\dot{y}_2 y_3 - \dot{y}_3 y_2}{\dot{y}_1 y_3 - \dot{y}_3 y_1}\right)' \\ &= \frac{(\ddot{y}_2 y_3 - \ddot{y}_3 y_2)(\dot{y}_1 y_3 - \dot{y}_3 y_1) - (\dot{y}_2 y_3 - \dot{y}_3 y_2)(\ddot{y}_1 y_3 - \ddot{y}_3 y_1)}{(\dot{x}_1 y_3^2)^2} \\ &= \frac{1}{(\dot{x}_1 y_3^2)^2} \begin{vmatrix} y_1 & y_2 & y_3 \\ \dot{y}_1 & \dot{y}_2 & \dot{y}_3 \\ \ddot{y}_1 & \ddot{y}_2 & \ddot{y}_3 \end{vmatrix}. \end{aligned} \tag{2.34}$$

Substituting (2.34) into (2.33) and using (2.32) (recall that $y(s) = 0$ is the origin) gives the curvature of Γ_+:

$$\kappa(t) = \frac{\Phi(t,s)}{y_3^4(t)\left(\dot{x}_1^2(t) + \dot{x}_2^2(t)\right)^{3/2}}. \tag{2.35}$$

By the properties of $C(s, q_{max}(s))$ mentioned prior to this proposition, $y_3(t) \neq 0, t \in (s, q_{max}(s))$. Also, $y_3(s) = 0$ and, if $H(s, q_{max}(s))$ is maximal, $y_3(q_{max}(s)) = 0$. It remains to show that $\dot{x}_1^2(t) + \dot{x}_2^2(t) \neq 0$. This would also imply that Γ_+ is smooth. We argue by contradiction. Suppose $\dot{x}_1(t) = \dot{x}_2(t) = 0$. Then $\dot{y}_2 y_3 = \dot{y}_3 y_2$, $\dot{y}_1 y_3 = \dot{y}_3 y_1$. Consequently, $y(t) \times \dot{y}(t)$ is parallel to the x_3-axis. Thus, either both $y(t)$ and $\dot{y}(t)$ are parallel to $DP_+(s)$ or $y(t)$ and $\dot{y}(t)$ are parallel to each other. Both cases are impossible because of the convexity of $\hat{C}(s, q_{max}(s))$ (cf. Proposition 2.3.1). Since $\Phi(t,s) \neq 0$ for $t \in [s, q_{max}(s)]$ (cf. Proposition 2.1.1), the desired assertion is proven. □

Denote $L_0^+ := DP_+(s) \cap \Pi_{osc}(s)$. It is clear that L_0^+ is an asymptote of Γ_+: $\mathrm{dist}(\hat{y}(t), L_0^+) \to 0$ as $t \to s^+$. Similarly, $L_0^- := DP_-(s) \cap \Pi_{osc}(s)$ is an asymptote of Γ_-: $\mathrm{dist}(\hat{y}(t), L_0^-) \to 0$ as $t \to s^-$.

Fix $x \in U$, which admits a PI-line. Let $I_{PI}(x) = [s_b(x), s_t(x)]$ be the PI-interval of x. Let $\hat{x}$ denote the projection of x onto a detector plane. Frequently it is convenient to identify detector planes by introducing systems of coordinates that depend smoothly on s. This allows to identify all $DP_+(s)$ and, separately, all $DP_-(s)$. Since $x \in U$, x does not belong to any plane passing through $y(s)$ and parallel to $DP_+(s)$ or $DP_-(s)$, where $s \in I_{PI}(x)$. Hence propositions 2.3.2 and 2.2.2 immediately imply the following statement.

Corollary 2.3.2. *As s moves along $I_{PI}(x)$, the point $\hat{x}$ traces smooth curves on $DP_+(s)$ and $DP_-(s)$. $\hat{x}$ is between $\Gamma_+(s)$ and L_0^+ on $DP_+(s)$ if and only if $s \in (s_b(x), s^*(x))$, and $\hat{x}$ is between L_0^- and $\Gamma_-(s)$ on $DP_-(s)$ if and only if $s \in (s^*(x), s_t(x))$.*

Loosely speaking, Corollary 2.3.2 can be stated as follows: $\hat{x}$ is between $\Gamma_+(s)$ and $\Gamma_-(s)$ if and only if $s \in I_{PI}(x)$.

Following [Kat02a, Kat04b], choose any $\psi \in C^\infty(\mathbb{R}^+)$ with the properties

$$\begin{aligned} &\psi(0) = 0;\ 0 < \psi'(t) < 1,\ t \geq 0, \\ &\psi'(0) = 0.5;\ \psi^{(2k+1)}(0) = 0,\ k \geq 1. \end{aligned} \tag{2.36}$$

Suppose s, s_1, and s_2 are related by

$$s_1 = \begin{cases} \psi(s_2 - s) + s, & s_2 \geq s, \\ \psi(s - s_2) + s_2, & s_2 < s. \end{cases} \tag{2.37}$$

¿From (2.36), $s_1 = s_1(s, s_2)$ is a C^∞ function of s and s_2. Conditions (2.36) are easy to satisfy. One can take, for example, $\psi(t) = t/2$, and this leads to

$$s_1 = (s + s_2)/2. \tag{2.38}$$

Denote also

$$\begin{aligned} u(s, s_2) &= \frac{(y(s_1) - y(s)) \times (y(s_2) - y(s))}{|(y(s_1) - y(s)) \times (y(s_2) - y(s))|} \mathrm{sgn}(s_2 - s), \\ &\qquad q_{min}(s) < s_2 < q_{max}(s), s_2 \neq s, \\ u(s, s_2) &= \frac{\dot{y}(s) \times \ddot{y}(s)}{|\dot{y}(s) \times \ddot{y}(s)|},\ s_2 = s. \end{aligned} \tag{2.39}$$

In the same way as in [Kat04b], we prove that $u(s, s_2)$ is a C^∞ vector function of its arguments. Let $\Pi(s, s_2)$ be the plane through $y(s), y(s_2)$, and $y(s_1(s, s_2))$. Intersection of $\Pi(s, s_2)$

with $DP_+(s)$ if $s < s_2 < q_{max}(s)$ or with $DP_-(s)$ if $q_{min}(s) < s_2 < s$ is called a filtering line and denoted $L(s, s_2)$.

Fix $x \in U$, which admits a PI-line, and $s \in I_{PI}(x)$. Find $s_2 \in I_{PI}(x)$ such that $\Pi(s, s_2)$ contains x. More precisely, we have to solve for s_2 the following equation

$$(x - y(s)) \cdot u(s, s_2) = 0, \ \ s_2 \in I_{PI}(x). \tag{2.40}$$

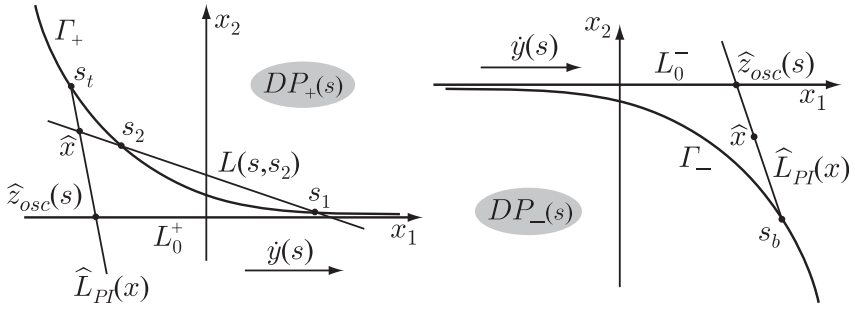

Figure 2.6: Detector planes $DP_+(s)$ (left panel) and $DP_-(s)$ (right panel).

Recall that $\dot{y}(s)$ is parallel to $DP_+(s)$ and $DP_-(s)$. For convenience, we choose the x_1- and x_2-axes so that

1. $\dot{y}(s)$ and the x_1-axis are parallel and point in the same direction;

2. The equation of $\Pi_{osc}(s)$ is $x_2 = 0$;

3. On $DP_+(s)$, Γ_+ is located in the half-plane $x_2 > 0$;

4. On $DP_-(s)$, Γ_- is located in the half-plane $x_2 < 0$.

Figure 2.6 illustrates the two detector planes.

The advantage of planes $DP_+(s)$ and $DP_-(s)$ is that the segments $C(s, q_{max}(s))$ and $C(q_{min}(s), s)$ are projected onto them as continuous curves with positive curvature. If C is a helix, the two segments become the usual 2π-segments $C(s, s+2\pi)$ and $C(s-2\pi, s)$. This makes it very convenient when describing how to choose filtering lines in a shift-invariant FBP algorithm. On the other hand, the disadvantage is that the two segments are projected onto two different planes. This makes it difficult to adapt the proofs from [Kat04b, Kat02a] to the present more general situation. Fortunately, the difficulty can be resolved. Given $x \in U$ with the PI-interval $I_{PI}(x) = [s_b(x), s_t(x)]$, we can find a family of "detector planes" such that for any $s \in I_{PI}(x)$ the entire PI-segment of x, $C(s_b(x), s_t(x))$, projects onto them in exactly the same way as in the case of a regular constant pitch helix. There is no guarantee that the larger segment $C(q_{min}(s), q_{max}(s))$ (which is equivalent to two adjacent turns of a helix) projects well onto the planes, but this is not needed.

Let $DP(s), s \in I_{PI}(x)$, be a plane not passing through $y(s)$ and parallel to $\dot{y}(s)$ and $N_{max}(s_b(x))$. Using the convexity of $C(s_b(x), s_t(x)) \subset C(s_b(x), q_{max}(s_b(x)))$ (cf. proposition 2.3.1 and Figure 2.5) and repeating the proof of proposition 2.3.3, we establish that the stereographic projection of $C(s_b(x), s_t(x))$ onto $DP(s)$ has all the usual properties as in the constant-pitch helix case. More precisely, the projections of $C(s_b(x), s)$ and $C(s, s_t(x))$ are concave down and up, respectively, they share the usual asymptote $DP(s) \cap \Pi_{osc}(s)$, are located on the opposite sides of the latter, etc. Thus, using the same argument as in [Kat04b, KBH04], we immediately obtain the following result.

Proposition 2.3.4. *The solution s_2 to (2.40) exists, is unique, and depends smoothly on s.*

The following result shows that filtering lines are shared by sufficiently many points $x \in U$. The planes $DP(s)$ used for the proof of proposition 2.3.4 are selected separately for each x, so they do necessarily work for all x in a large subset of U. Thus we have to go back to the planes $DP_+(s)$ and $DP_-(s)$.

Proposition 2.3.5. *All $x \in U$ that project onto any line $L(s, s_2), s < s_2 < q_{max}(s)$, on $DP_+(s)$ to the left of s_2 or onto $L(s, s_2), q_{min}(s) < s_2 < s$, on $DP_-(s)$ to the right of s_2, share $L(s, s_2)$ as their filtering line.*

Proof. We only consider the case when $s_2 > s$, i.e. $\hat{x} \in DP_+(s)$. The other case can be considered analogously. We have $s_t(x) \in \Gamma_+$. By corollary 2.3.2, $\hat{x}$ appears between L_0^+ and Γ_+. From the proof of proposition 2.3.1, $\Pi_{osc}(s)$ intersects the PI-segment of x, $H(s_b(x), s_t(x))$. Let $z_{osc}(x)$ denote the point of intersection. Let $\Pi_{max}(s)$ be the plane through $y(s)$ and parallel to $\dot{y}(s)$ and $N_{max}(s)$. The intersection of the line through $L_{PI}(x)$ and $\Pi_{max}(s)$ is denoted $z_{max}(s)$. Clearly, $z_{osc}(s) = z_{max}(s)$ when $s = s_b(x)$. From the proof of proposition 2.3.2, $z_{osc}(s)$ moves toward $y(s_t(x))$ along $L_{PI}(x)$ as s increases from $s_b(x)$ to $s_t(x)$. From the convexity of $\hat{C}(s, q_{max}(s))$ (cf. Figure 2.5), it is easy to obtain that in a neighborhood of $s = s_b(x)$ the point $z_{max}(s)$ moves away from $H(s_b(x), s_t(x))$ as s increases. If for some $s \in (s_b(x), s_t(x))$ the points $z_{osc}(x)$ and $y(s_t(x))$ are on the opposite sides of $\Pi_{max}(s)$, then the point $z_{max}(s)$ enters the line segment $[z_{osc}(x), y(s_t(x))]$ for some $s = s_0 \in (s_b(x), s_t(x))$. Hence, either (i) $z_{osc}(s_0) = z_{max}(s_0)$ or (ii) $y(s_t(x)) = z_{max}(s_0)$. From proposition 2.1.1, $[y(q_{max}(s_0)) - y(s_0), \dot{y}(s_0), \ddot{y}(s_0)] \neq 0$, so (i) implies that $z_{osc}(s_0) - y(s_0)$

and $\dot{y}(s_0)$ are collinear, which contradicts corollary 2.3.1. In case (ii), $y(s_t(x)) \in \Pi_{max}(s_0)$, which contradicts the containment property.

Hence $\hat{L}_{PI}(x)$, the projection of $H(s_b(x), s_t(x))$ onto $DP_+(s)$, intersects L_0^+. More precisely, the projection of the line segment $[z_{osc}(x), y(s_t(x))] \subset L_{PI}(x)$ is a continuous line segment that connects Γ_+ and L_0^+ (see Figure 2.6). Note that proposition 2.3.2 implies $z \in [z_{osc}(x), y(s_t(x))]$ if $s < s^*(x)$. It turns out that $\hat{L}_{PI}(x)$ does not intersect Γ_+ at any point other than $s_t(x)$. Suppose there is an additional intersection point t. Thus the plane through $y(s)$ and $H(s_b(x), s_t(x))$ intersects $C_{PI}(x)$ at four points: $s_b(x), t, s$, and $s_t(x)$, and this contradicts corollary 2.1.1.

If x projects onto $L(s, s_2)$ to the left of s_2, we make two observations: (i) $\hat{x}$ is between L_0^+ and Γ_+ on $DP_+(s)$; and (ii) $s_2 < s_t$ (due to the properties of $\hat{L}_{PI}(x)$ that we just established). From (i) and corollary 2.3.2, $s \in I_{PI}(x)$. From (ii), $s_2 \in (s, s_t(x))$, so by (i) $s_2 \in I_{PI}(x)$. By construction, s_2 was chosen to satisfy (2.36), (2.37) and $(x - y(s)) \cdot u(s, s_2) = 0$. We have just shown that $s, s_2 \in I_{PI}(x)$. This proves that $L(s, s_2)$ is the filtering line for x. □

By proposition 2.3.5, our construction defines $s_2 := s_2(s, x)$ and, consequently, $u(s, x) := u(s, s_2(s, x))$. Let $D_f(s, \Theta) = \int_0^\infty f(y(s) + t\Theta)dt$, $|\Theta| = 1$, denote the cone beam transform of f. The main result of this chapter is the following theorem.

Theorem 2.3.1. *Let C be a curve (2.1), which satisfies conditions C1–C4. Let $I_0 \subset I$ be an interval, such that the set U defined by (2.27) is non-empty. For any $f \in C_0^\infty(U)$ and*

$x \in U$ which admits a PI line one has

$$f(x) = -\frac{1}{2\pi^2} \int_{I_{PI}(x)} \frac{1}{|x - y(s)|} \int_0^{2\pi} \frac{\partial}{\partial q} D_f(q, \Theta(s, x, \gamma))\Big|_{q=s} \frac{d\gamma}{\sin\gamma} ds, \tag{2.41}$$

where $e(s, x) := \beta(s, x) \times u(s, x)$ *and* $\Theta(s, x, \gamma) := \cos\gamma\beta(s, x) + \sin\gamma e(s, x)$.

Proof. Corollaries 2.1.1, 2.1.2, 2.3.2, and Propositions 2.3.1, 2.3.2, 2.3.3, and 2.3.4 imply that locally, i.e. in a neighborhood of $I_{PI}(x)$, the curve C behaves in essentially the same way as the usual helix. Hence the same argument as in [Kat04b, KBH04] can be used to prove that (2.41) holds. □

Proposition 2.3.5 implies that (2.41) is of the efficient shift-invariant FBP form.

2.4 Numerical experiments

Numerical experiments are conducted using flat detector geometry. The simulation parameters are summarized in Table 2.1. The algorithm is implemented in the native coordinates following [NPH03]. We use the virtual detector, which always contains the x_3-axis. The clock phantom (see, e.g., [KBH04]) is chosen for reconstruction. The background cylinder is at 0 HU, the spheres are at 1000 HU, and the air is at -1000 HU.

Two source trajectories have been used. The first one is a variable radius helix given by the formula:

$$y(s) = \left(R(s)\cos s, R(s)\sin s, \frac{h_0}{2\pi} s \right), \; R(s) = R(1 + 0.3\sin(s/3)), \tag{2.42}$$

Table 2.1: Simulation parameters

Parameter	Value	Units
Views per rotation	1000	
Number of detector columns	1201	
Number of detector rows	161	
Detector pixel size	0.5×0.5	mm^2

where $R = 600$mm, and table feed per turn is $h_0 = 35$mm. The projection of this trajectory onto the plane $x_3 = 0$ for $s \in [-2\pi, 2\pi]$ is shown in Fig. 2.7. The boundary of the set U

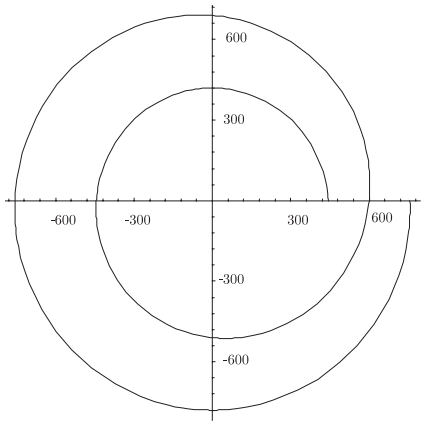

Figure 2.7: Projection of the source trajectory in (2.42) onto the xy-plane.

is calculated according to (2.27). The cross-section of the boundaries of cylinders $Cyl_{min}(s)$ and $Cyl_{max}(s)$ with the plane $x_3 = 0$ is shown in Fig. 2.9 (left panel). The solid circle of radius $r = 240$mm shows the boundary of the clock phantom, and the dashed circle is of the maximum radius $r \approx 374$mm that fits inside the cross-section of U. The result of reconstruction is shown in Fig. 2.8.

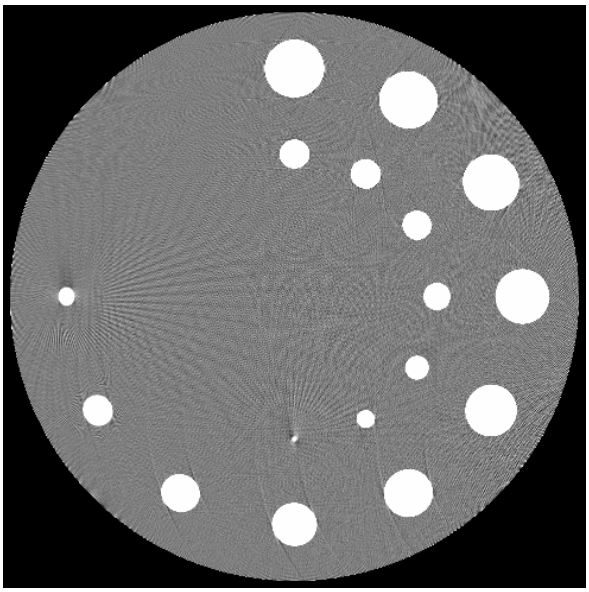

Figure 2.8: Reconstruction of the clock phantom from trajectory (2.42): slice $x_3 = 0$, WL=0 HU, WW=100 HU.

The second experiment is carried out using the variable radius and variable pitch helix given by:

$$y(s) = \left(R(s)\cos s, R(s)\sin s, \frac{h(s)}{2\pi} s \right), \; h(s) = h_0 \left(1 + \frac{\sin(s/2)}{s} \right). \tag{2.43}$$

Here $R(s)$ and h_0 are the same as in (2.42). The cross-section of the boundaries of cylinders $Cyl_{min}(s)$ and $Cyl_{max}(s)$ with the plane $x_3 = 0$ is shown in Fig. 2.9 (right panel). Again, the solid circle of radius $r = 240$mm shows the boundary of the clock phantom, and the dashed circle is of the maximum radius $r \approx 348$mm that fits inside the cross-section of U. The results of the reconstruction are shown in Fig. 2.10.

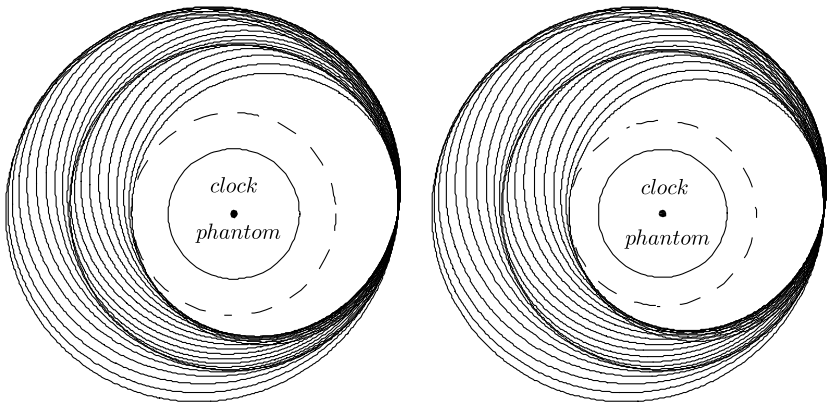

Figure 2.9: Cross-section of boundaries of cylinders $Cyl(s)$ from (2.27) for trajectory (2.42) (left panel) and trajectory (2.43) (right panel).

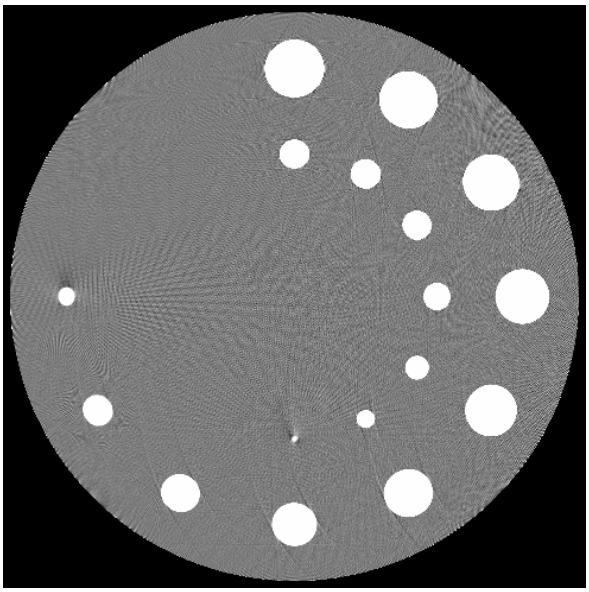

Figure 2.10: Reconstruction of the clock phantom from trajectory (2.43): slice $z = 0$, WL=0 HU, WW=100 HU.

APPENDIX. ADDITIONAL PROOFS

A.1 Proof of Propositions 1.5.1, 1.5.2, and 1.5.3

We need an auxiliary result for the following proofs.

Proposition A.1.1. *Let L be a line on $DP(s)$, which is tangent to $\hat{C}$ at a point $\hat{y}(q)$, where $\hat{C}$ has zero curvature. Then $\Pi_{osc}(q)$ contains $y(s)$, and L is the intersection of $\Pi_{osc}(q)$ with $DP(s)$.*

Proof. Consider the plane determined by L and $y(s)$. A short calculation shows that

$$[y(q) - y(s), \dot{y}(q), \ddot{y}(q)] = \Phi(q, s). \tag{A.1}$$

By assumption, the curvature of $\hat{C}$ at $\hat{y}(q)$ equals zero. So $\Phi(q, s) = 0$, and the assertion immediately follows. □

Proof of Proposition 1.5.1. The statement of the proposition can be reformulated in the following way: for all chords $H(s_0, s_1), 0 < s_1 - s_0 < 2\pi$, passing through U_0 and for all $s \in (s_0, s_1)$, any plane containing $H(s_0, s_1)$ and $y(s)$ has only three intersections with C inside the interval $(s - 2\pi, s + 2\pi)$. Suppose this is not true. Pick $x_0 \in U_0$ with the PI line $H(s_0, s_1)$ such that the plane Π_0 through $H(s_0, s_1)$ and $y(s)$ intersects C inside $(s - 2\pi, s + 2\pi)$ at least five times (since $y(s - 2\pi)$ and $y(s + 2\pi)$ are on opposite sides of Π_0, the number of IPs is odd). As is easily seen, by a rotation of Π_0 about $H(s_0, s_1)$ we can produce a plane Π_0' with the following properties: (1) Π_0' contains $H(s_0, s_1)$, (2) Π_0' intersects C at $y(p)$, and (3) Π_0' touches C at $y(q)$, where p, q are some points such that $\max(s_0, s_1, p, q) - \min(s_0, s_1, p, q) < 2\pi$. The direction of rotation is determined by a pair of

IPs not separated by s_0 and s_1. We can rotate Π_0 in such a way that the two IPs collide and produce the point of tangency $y(q)$. Note that if the pair of IPs was inside $[s_0, s_1]$, then q will be inside the interval. Similarly, if the pair of IPs was outside $[s_0, s_1]$, then q will be outside the interval. Note that q cannot be in the interior of $[s_0, s_1]$, because this would mean that the T and A curves of x_0 intersect. So we assume that q is outside of $[s_0, s_1]$. In order to establish the inequalities given above, we note the following property of C: if a plane passes through two points $y(s_1)$ and $y(s_2)$ on C such that $|s_1 - s_2| = 2\pi$, then the plane is necessarily vertical. Thus, since the tangency is achieved before the plane becomes vertical, the third IP does not leave $(s_1 - 2\pi, s_0 + 2\pi)$.

Now pick a point $x_1 \in U_0$ such that all planes through the PI line of x_1 intersect C no more than three times (such a point exists since one only needs to make sure that the endpoints of the PI line are sufficiently far from $[A, B]$ for the point to satisfy this property). Choose a continuous path $x(t)$ connecting x_0 and x_1, which is inside U_0. By construction, there must be a point $x(t^*)$ on the path where at least one of the following events occurs: (a) p collides with either s_0 or s_1, (b) q collides with either s_0 or s_1, (c) p and q collide. In case (a) we get a contradiction in the following way. Without loss of generality, assume that p collided with s_1 (the other case can be considered analogously). Since $q \notin [s_0, s_1]$, we need to consider the following two cases:

1. $q < s_0 < s_1 = p$. In this case the critical chord $H(p, q)$ spans an arc of C greater than the arc spanned by $H(s_0, s_1)$, so the latter chord cannot intersect U_0. Here we have used condition 2 and the assumption that U_0 is a cylinder inside U_{PI}.

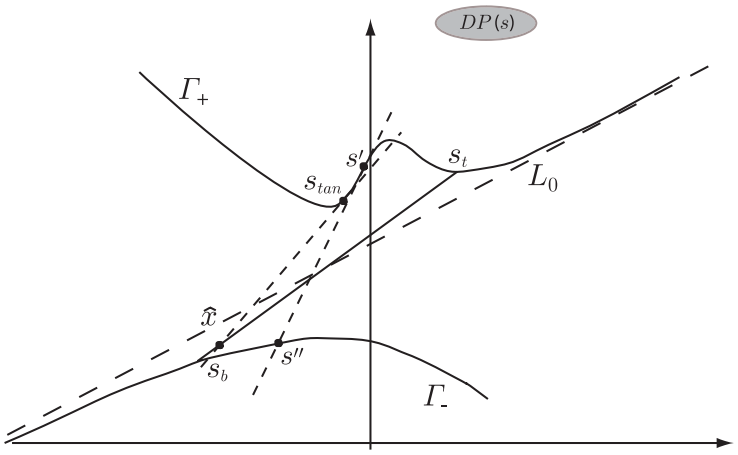

Figure A.1: Construction of the chord $H(s', s'')$

2. $s_0 < s_1 = p < q$. One sees that the projection of $H(p, q)$ onto $DP(s_0)$ is tangent to $\hat{C}$ at the endpoints p and q, and both are located on Γ_+. Thus there is necessarily a point of zero curvature $s' \in [p, q]$, i.e. $\Pi_{osc}(s')$ intersects C at s_0 (cf. Proposition A.1.1). Therefore the chord $H(s_0, s')$ belongs to the boundary of U'. Since $s' > p = s_1$, it spans an arc of C greater than the arc spanned by $H(s_0, s_1)$. Using that U_0 is a cylinder inside U', we see that $H(s_0, s_1)$ cannot intersect U_0.

In the remaining cases (b) and (c) we get a contradiction as well using the property that $H(s_0, s_1)$ belongs to an osculating plane. □

Proof of Proposition 1.5.2. Pick $s \in I_{PI}(x)$. Suppose there exists a line tangent to Γ_+ at s_{tan} and passing through $\hat{x}$ such that $s_{tan} \notin I_{PI}(x)$, but the point of tangency lies to the right of $\hat{x}$ on $DP(s)$ (the other case when the tangency is on Γ_- can be considered analogously). Since a curve with curvature of constant sign would stay on the same side of a tangent (this is not

true in general, but holds for Γ_- and Γ_+), there exists $s' \notin I_{PI}(x)$ such that the curvature of Γ_+ at s' is zero and the line tangent to Γ_+ at $\hat{y}(s')$ intersects the line segment $\hat{L}_{PI}(x)$ (see Figure A.1). One sees from the projection onto $DP(s)$ that since $s' \notin I_{PI}(x)$, the line necessarily intersects Γ_- at some $\hat{y}(s'')$, and s'' is to the left of $I_{PI}(x)$ (see Figure A.1). Due to Proposition A.1.1 above, $\Pi_{osc}(s')$ intersects the helix at $y(s)$. Since it also intersects the helix at $y(s'')$, $H(s', s'')$ belongs to the boundary of U'. Since it spans the arc greater than that spanned by $L_{PI}(x)$, this immediately implies that $x \notin U_0$ due to the assumption that no boundary chord spans an arc greater than π. □

Proof of Proposition 1.5.3. We first note that by Proposition 1.5.2, the point of tangency is necessarily inside $I_{PI}(x)$ for $\hat{e}_j(s, x)$, $j = 1, 2, 3$. Considering the possible projections of the helix in Figures 1.6 and 1.7, one sees that if the slope of $\hat{L}_{PI}(x)$ is greater than the slope of any of $\hat{e}_j(s, x)$, $j = 0, 1, 2, 3$, then $\hat{L}_{PI}(x)$ necessarily intersects $\hat{C}$ more than twice, which contradicts Proposition 1.5.1. □

LIST OF REFERENCES

[BKP05] C. Bontus, T. Köhler, and R. Proksa, *EnPiT: filtered back-projection algorithm for helical CT using an n-Pi acquisition*, IEEE Transactions on Medical Imaging **24** (2005), 977–986.

[CZLN06] G.-H. Chen, T.-L. Zhuang, S. Leng, and B. E. Nett, *Shift-invariant and mathematically exact cone-beam FBP reconstruction using a factorized weighting function*, IEEE Transactions on Medical Imaging (2006), submitted.

[Kat02a] A. Katsevich, *Analysis of an exact inversion algorithm for spiral cone-beam CT*, Physics in Medicine and Biology **47** (2002), 2583–2598.

[Kat02b] _____, *Theoretically exact filtered backprojection-type inversion algorithm for Spiral CT*, SIAM Journal on Applied Mathematics **62** (2002), 2012–2026.

[Kat03] _____, *A general scheme for constructing inversion algorithms for cone beam CT*, International Journal of Mathematics and Mathematical Sciences **21** (2003), 1305–1321.

[Kat04a] _____, *Image reconstruction for the circle and line trajectory*, Physics in Medicine and Biology **49** (2004), 5059–5072.

[Kat04b] _____, *An improved exact filtered backprojection algorithm for spiral computed tomography*, Advances in Applied Mathematics **32** (2004), 681–697.

[Kat04c] _____, *On two versions of a 3π algorithm for spiral CT*, Physics in Medicine and Biology **49** (2004), 2129–2143.

[Kat05] _____, *Image reconstruction for the circle and arc trajectory*, Physics in Medicine and Biology **50** (2005), 2249–2265.

[Kat06] _____, *3PI algorithms for helical computer tomography*, Advances in Applied Mathematics **21** (2006), 213–250.

[KBH04] A. Katsevich, Samit Basu, and Jiang Hsieh, *Exact filtered backprojection reconstruction for dynamic pitch helical cone beam computed tomography*, Physics in Medicine and Biology **49** (2004), 3089–3103.

[KBK06] Th. Köhler, C. Bontus, and P. Koken, *The Radon-split method for helical cone-beam CT and its application to nongated reconstruction*, IEEE Transactions on Medical Imaging **25** (2006), 882–897.

[KK] M. Kapralov and A. Katsevich, *A general scheme for constructing inversion algorithms for the cone beam transform*, in preparation.

[KK06a] ———, *A 1PI algorithm for helical trajectories that violate the convexity condition*, Inverse Problems **22** (2006), 2123–2143.

[KK06b] A. Katsevich and M. Kapralov, *Efficient inversion of the cone beam transform for a general class of curves*, (submitted).

[KL03] A. Katsevich and G. Lauritsch, *Filtered backprojection algorithms for spiral cone beam CT*, Sampling, Wavelets, and Tomography (John Benedetto and Ahmed Zayed, eds.), Birkhauser, 2003, pp. 255–287.

[KND00] H. Kudo, F. Noo, and M. Defrise, *Quasi-exact filtered backprojection algorithm for long-object problem in helical cone-beam tomography*, IEEE Transactions on Medical Imaging **19** (2000), 902–921.

[NPH03] F. Noo, J. Pack, and D. Heuscher, *Exact helical reconstruction using native cone-beam geometries*, Physics in Medicine and Biology **48** (2003), 3787–3818.

[PN05] J. D. Pack and F. Noo, *Cone-beam reconstruction using 1D filtering along the projection of M-lines*, Inverse Problems **21** (2005), 1105–1120.

[PNC05] J. D. Pack, F. Noo, and R. Clackdoyle, *Cone-beam reconstruction using the backprojection of locally filtered projections*, IEEE Transactions on Medical Imaging **24** (2005), 1–16.

[SZP05] E.Y. Sidky, Y. Zou, and X. Pan, *Minimum data image reconstruction algorithms with shift-invariant filtering for helical, cone-beam CT*, Physics in Medicine and Biology **50** (2005), 1643–1657.

[YLKK06] H. Yang, M. Li, K. Koizumi, and H. Kudo, *Exact cone beam reconstruction for a saddle trajectory*, Physics in Medicine and Biology **51** (2006), 1157–1172.

[YW04] H. Yu and G. Wang, *Studies on implementation of the Katsevich algorithm for spiral cone-beam CT*, Journal of x-ray science and technology **12** (2004), 97–116.

[YZW04a] Y. Ye, J. Zhu, and G. Wang, *Geometric studies on variable radius spiral cone-beam scanning*, Medical Physics **31** (2004), 1473–1480.

[YZW04b] ———, *Minimum detection windows, pi-line existence and uniqueness for helical cone-beam scanning of variable pitch*, Medical Physics **31** (2004), 566–572.

[YZYW05a] Y. Ye, S. Zhao, H. Yu, and G. Wang, *A general exact reconstruction for cone-beam CT via backprojection-filtration*, IEEE Transactions on Medical Imaging **24** (2005), 1190–1198.

[YZYW05b] H. Yu, S. Zhao, Y. Ye, and G. Wang, *Exact BPF and FBP algorithms for nonstandard saddle curves*, Medical Physics **32** (2005), 3305–3312.

[ZLNC04] T. Zhuang, S. Leng, B. E. Nett, and G. Chen, *Fan-beam and cone-beam image reconstruction via filtering the backprojection image of differentiated projection data*, Physics in Medicine and Biology **49** (2004), 1643–1657.

[ZPXW05] Y. Zou, X. Pan, D. Xia, and G. Wang, *PI-line-based image reconstruction in helical cone-beam computed tomography with a variable pitch*, Medical Physics **32** (2005), 2639–2648.